

Doubly Stochastic Subspace Clustering

Derek Lim

Department of Computer Science
Cornell University
dl772@cornell.edu

René Vidal

Mathematical Institute for Data Science
Johns Hopkins University
{rvidal, bhaeffele}@jhu.edu

Benjamin D. Haeffele

Abstract

Many state-of-the-art subspace clustering methods follow a two-step process by first constructing an affinity matrix between data points and then applying spectral clustering to this affinity. Most of the research into these methods focuses on the first step of generating the affinity, which often exploits the self-expressive property of linear subspaces, with little consideration typically given to the spectral clustering step that produces the final clustering. Moreover, existing methods often obtain the final affinity that is used in the spectral clustering step by applying ad-hoc or arbitrarily chosen postprocessing steps to the affinity generated by a self-expressive clustering formulation, which can have a significant impact on the overall clustering performance. In this work, we unify these two steps by learning both a self-expressive representation of the data and an affinity matrix that is well-normalized for spectral clustering. In our proposed models, we constrain the affinity matrix to be doubly stochastic, which results in a principled method for affinity matrix normalization while also exploiting known benefits of doubly stochastic normalization in spectral clustering. We develop a general framework and derive two models: one that jointly learns the self-expressive representation along with the doubly stochastic affinity, and one that sequentially solves for one then the other. Furthermore, we leverage sparsity in the problem to develop a fast active-set method for the sequential solver that enables efficient computation on large datasets. Experiments show that our method achieves state-of-the-art subspace clustering performance on many common datasets in computer vision.

1. Introduction

Subspace clustering seeks to cluster a set of data points that are approximately drawn from a union of low dimensional linear (or affine) subspaces into clusters, where each linear (or affine) subspace defines a cluster (i.e., every point in a given cluster lies in the same subspace) [41]. The most common class of subspace clustering algorithms for cluster-

ing a set of n data points proceed in two stages: 1) Learning an affinity matrix $\mathbf{A} \in \mathbb{R}^{n \times n}$ that defines the similarity between pairs of datapoints; 2) Applying a graph clustering technique, such as spectral clustering [43, 39], to produce the final clustering. In particular, arguably the most popular model for subspace clustering is to construct the affinity matrix by exploiting the ‘self-expressive’ property of linear (or affine) subspaces, where a point within a given subspace can be represented as a linear combination of other points within the subspace [10, 11, 30, 52, 53, 41]. For a dataset $\mathbf{X} \in \mathbb{R}^{d \times n}$ of n , d -dimensional data points, this is typically captured by an optimization problem of the form:

$$\min_{\mathbf{C}} \frac{1}{2} \|\mathbf{X} - \mathbf{X}\mathbf{C}\|_F^2 + \lambda \theta(\mathbf{C}), \quad (1)$$

where the first term captures the self-expressive property, $\mathbf{X} \approx \mathbf{X}\mathbf{C}$, and the second term, θ , is some regularization term on \mathbf{C} to encourage that a given point is primarily represented by other points from its own subspace and to avoid trivial solutions such as $\mathbf{C} = \mathbf{I}$. Once the self-expressive representation \mathbf{C} has been learned from (1), the final affinity \mathbf{A} is then typically constructed by rectifying and symmetrizing \mathbf{C} , e.g., $\mathbf{A} = (|\mathbf{C}| + |\mathbf{C}^\top|)/2$.

However, as we detail in Section 2.1 and illustrate in Figure 1, many subspace clustering methods require ad-hoc or unjustified postprocessing procedures on \mathbf{C} to work in practice. These postprocessing steps serve to normalize \mathbf{C} to produce an affinity \mathbf{A} with better spectral clustering performance, but they add numerous arbitrary hyperparameters to the models and receive little mention in the associated papers. Likewise, it is well-established that some form of Laplacian normalization is needed for spectral clustering to be successful [43], for which the practitioner again has multiple choices of normalization strategy.

In this paper, we propose a new subspace clustering framework which explicitly connects the self-expressive step, the affinity normalization, and the spectral clustering step. We develop novel scalable methods for this framework that address issues with and empirically outperform other subspace clustering models. To motivate our proposed models, we first discuss the desired properties of subspace

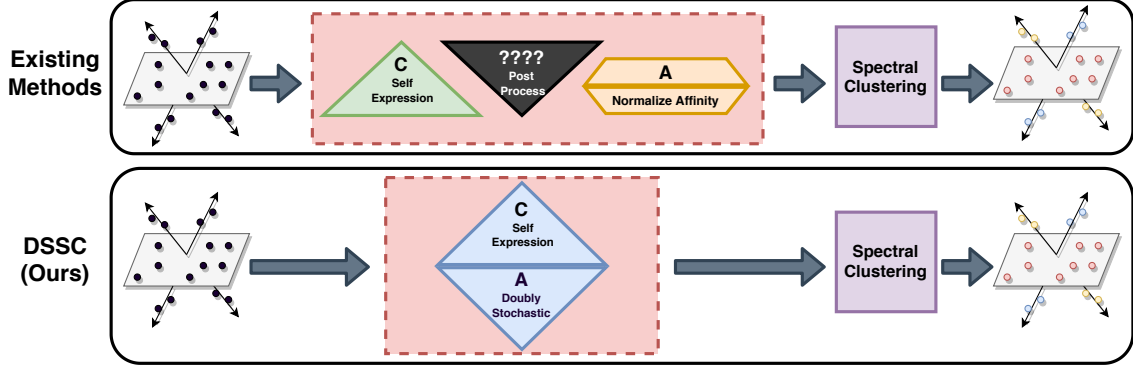


Figure 1. Diagram comparing our DSSC framework with existing methods for self-expressive affinity-based subspace clustering. (Top row) Most existing methods focus on computing the self-expressive matrix \mathbf{C} , but they are also reliant on choices of postprocessing and affinity normalization, which often take the form of ad-hoc procedures that are not well-studied. (Bottom row) Our DSSC models learn a doubly stochastic affinity matrix $\mathbf{A} \in \Omega_n$ along with the self-expressive matrix \mathbf{C} . The doubly stochastic affinity does not require postprocessing or normalization to be used for spectral clustering and has numerous desirable properties for subspace clustering.

clustering affinities that one would like for successful spectral clustering. Specifically, we desire affinities \mathbf{A} that have the following properties:

- (A1) *Well-normalized for spectral clustering.* We should better leverage knowledge that \mathbf{A} will be input to spectral clustering. Many forms of ad-hoc postprocessing in subspace clustering perform poorly-justified normalization, and there is also a choice of normalization to be made in forming the graph Laplacian [43].
- (C1) *Sparsity.* Much success in subspace clustering has been found with enforcing sparsity on \mathbf{C} [10, 11, 53]. In particular, many sparsity-enforcing methods are designed to ensure that the nonzero entries of the affinity matrix correspond to pairs of points which belong to the same subspace. This leads to high clustering accuracy, desirable computational properties, and provable theoretical guarantees.
- (C2) *Connectivity.* There should be sufficiently many edges in the underlying graph of \mathbf{A} so that all points within the same subspace are connected [32, 46, 52]. Thus, there is a trade-off between sparsity and connectivity that subspace clustering methods must account for.

Properties (C1) and (C2) are well studied in the subspace clustering literature, and can be enforced on the self-expressive \mathbf{C} , since rectifying and symmetrizing a \mathbf{C} with these properties, for example, maintains the properties. However, property (A1) must be enforced on \mathbf{A} ; thus, (A1) is often neglected in several aspects (see Section 2.1), and is mostly handled by ad-hoc postprocessing methods, if handled at all. In working towards (A1), we first constrain $\mathbf{A} \geq \mathbf{0}$, since nonnegativity of the affinity is necessary for interpretability and alignment with spectral clustering theory. Beyond this, spectral clustering also benefits from having rows and columns in the affinity matrix of the same scale, and many forms of Laplacian normalization for

spectral clustering normalize rows and/or columns to have similar scale [43]. In particular, one form of normalization that is well established in the spectral clustering literature is to constrain the rows and columns to have unit l_1 norm. Because \mathbf{A} is additionally constrained to be nonnegative, this is equivalent to requiring each row sum and column sum of \mathbf{A} to be 1, resulting in constraints that restrict the affinities \mathbf{A} to be in the convex set of doubly stochastic matrices [17]:

$$\Omega_n = \{\mathbf{A} \in \mathbb{R}^{n \times n} \mid \mathbf{A} \geq \mathbf{0}, \mathbf{A}\mathbf{1} = \mathbf{1}, \mathbf{A}^\top \mathbf{1} = \mathbf{1}\}. \quad (2)$$

Doubly stochastic matrices have been thoroughly studied for spectral clustering, and doubly stochastic normalization has been shown to significantly improve the performance of spectral clustering [54, 55, 45, 34, 15, 18, 44, 22, 48]. Moreover, doubly stochastic matrices are invariant to the most widely-used types of Laplacian normalization [43], which removes the need to choose a Laplacian normalization scheme. Further, the authors of [55] show that various Laplacian normalization schemes can be viewed as attempting to approximate a given affinity matrix with a doubly stochastic matrix under certain distance metrics.

Beyond being well-normalized for spectral clustering (A1), the family of doubly stochastic matrices can also satisfy properties (C1) and (C2). Our proposed methods will give control over the sparsity-connectivity trade-off through interpretable parameters, and we in practice learn \mathbf{A} that are quite sparse. Additionally, doubly stochastic matrices have a guarantee of a certain level of connectivity due to the row sum constraint, which prohibits solutions with all-zero rows (that can occur in other subspace clustering methods). The convexity of Ω_n along with the sparsity of our learned \mathbf{A} allow us to develop novel scalable algorithms for doubly stochastic projection and hence scalable methods for subspace clustering with doubly stochastic affinities.

Contributions. In this work, we develop a framework that

unifies the self-expressive representation step of subspace clustering with the spectral clustering step by formulating a model that jointly solves for a self-expressive representation \mathbf{C} and a doubly stochastic affinity matrix \mathbf{A} . While our general model is non-convex, we provide a convex relaxation that is provably close to the non-convex model and that can be solved by a type of linearized ADMM [31]. A closer analysis also allows us to formulate a sequential algorithm to quickly compute an approximate solution, in which we first efficiently learn a self-expressive matrix and then subsequently fit a doubly stochastic matrix by a regularized optimal transport problem [4, 28]. We leverage inherent sparsity in the problem to develop a scalable active-set method for computing in this sequential model. Finally, we validate our approach with experiments on various standard subspace clustering datasets, where we demonstrate that our models significantly improve on the current state-of-the-art in a variety of performance metrics.

1.1. Related Work

Self-expressive and Affinity Learning. Existing methods that have attempted to unify the self-expressive and spectral clustering steps in subspace clustering include: Structured SSC [25], which jointly learns a self-expressive representation and a binary clustering matrix, and Block Diagonal Representation [29] and SC-LALRG [50], which jointly learn a self-expressive representation and a constrained affinity for spectral clustering. However, all of these methods are non-convex, require iterative optimization methods, and necessitate expensive spectral computations in each iteration. As such, their scalability is greatly limited. In contrast, our methods have convex formulations, and we can compute the true minimizers very efficiently with our developed algorithms.

Doubly Stochastic Clustering. Doubly stochastic constraints have been used in standard spectral clustering methods where the input affinity is known, but they have not been used to directly learn an affinity matrix for a self-expressive representation, as is desired in subspace clustering.

Specifically, Zass and Shashua find strong performance by applying standard spectral clustering to the nearest doubly stochastic matrix to the input affinity in Frobenius norm [55]. Also, there has been work on learning doubly stochastic approximations of input affinity matrices subject to rank constraints [34, 45, 49]. Further, Landa *et al.* show that doubly stochastic normalization of the ubiquitous Gaussian kernel matrix by diagonal matrix scaling is robust to heteroskedastic additive noise on the data points [22].

To the best of our knowledge, only one subspace clustering method [24] utilizes doubly stochastic constraints, but they enforce very expensive semi-definite constraints, use ad-hoc non-convex postprocessing, and do not directly apply spectral clustering to the doubly stochastic matrix. In

contrast, we develop scalable methods with principled convex formulations that do not require postprocessing before applying spectral clustering.

Scalable Subspace Clustering. Existing methods or making subspace clustering scalable leverage sparsity in the self-expressive representation [6, 52, 9, 53], leverage structure in the final affinity [35, 2], and/or use greedy heuristics [9, 53, 51] to efficiently compute subspace clusterings. Our scalable method is able to exploit sparsity in both the self-expressive representation and affinity construction, is easily parallelizable (allowing a simple and fast GPU implementation), and is fully convex, with no use of greedy heuristics.

2. Doubly Stochastic Models

In this section, we further detail the motivation for learning doubly stochastic affinities for subspace clustering. Then we develop two models for subspace clustering with doubly stochastic affinities. Our J-DSSC model jointly learns a self-expressive matrix and doubly stochastic affinity, while our A-DSSC model is a fast approximation that sequentially solves for a self-expressive matrix and then a doubly stochastic affinity that approximates it.

2.1. Benefits of Doubly Stochastic Affinities

As discussed above, existing subspace clustering methods such as SSC [11], LRR [27], EDSC [19], and deep subspace clustering networks (DSC-Net) [20] require various ad-hoc postprocessing methods to achieve strong clustering performance on certain datasets. For example, it has recently been shown that if one removes the ad-hoc postprocessing steps from DSC-Net [20] then the performance drops considerably — performing no better than simple baseline methods and far below state-of-the-art [14]. Common postprocessing steps include keeping only the top l entries of each column of \mathbf{C} , normalizing columns of \mathbf{C} , and/or using SVD-based postprocessing, each of which introduces extra hyperparameters and degrees of freedom for the practitioner. Likewise, the practitioner is also required to make a choice on the particular type of Laplacian normalization to use [43].

To better connect the self-expressive step with the subsequent spectral clustering step and to avoid the need for ad-hoc postprocessing methods, we propose a framework for directly learning an affinity \mathbf{A} that already has desired properties (A1) and (C1)-(C2) for spectral clustering. Restricting $\mathbf{A} \in \Omega_n$ to be in the convex set of doubly stochastic matrices achieves these goals while allowing for highly efficient computation.

As noted in the introduction, doubly stochastic matrices are already nonnegative, so we do not need to take absolute values of some computed matrix. Also, each row and column of a doubly stochastic matrix sums to one, so they

each have the same scale in l_1 norm — removing the need to postprocess by scaling rows or columns. Importantly for (A1), doubly stochastic matrices are invariant to most forms of Laplacian normalization used in spectral clustering. For example, for a symmetric affinity matrix \mathbf{A} with row sums $\mathbf{D} = \text{diag}(\mathbf{A}\mathbf{1})$, widely used Laplacian variants include the unnormalized Laplacian $\mathbf{D} - \mathbf{A}$, the normalized Laplacian $\mathbf{I} - \mathbf{D}^{-1/2}\mathbf{A}\mathbf{D}^{-1/2}$, and the random walk Laplacian $\mathbf{I} - \mathbf{D}^{-1}\mathbf{A}$ [43]. When \mathbf{A} is doubly stochastic, the matrix of row sums satisfies $\mathbf{D} = \mathbf{I}$, so all of the normalization variants are equivalent and give the same Laplacian $\mathbf{I} - \mathbf{A}$.

In addition, many types of regularization and constraints that have been proposed for subspace clustering tend to desire sparsity (C1) and connectivity (C2), in the sense that they want \mathbf{A}_{ij} to be small in magnitude or zero when \mathbf{x}_i and \mathbf{x}_j belong to different subspaces and to be nonzero for sufficiently many pairs (i, j) where \mathbf{x}_i and \mathbf{x}_j belong to the same subspace [32, 46]. The doubly stochastic matrices learned by our models can be tuned to achieve any desired sparsity level. Also, doubly stochastic affinities are guaranteed a certain level of connectedness, as each row must sum to 1. This means that there cannot be any zero rows in the learned affinity, unlike in methods that compute representations one column at a time such as SSC [11], EnSC [52], and SSC-OMP [53], where it is possible that a point is never used in the self-expressive representation of other points.

2.2. Joint Learning: J-DSSC

In developing our model to jointly learn a self-expressive matrix and doubly stochastic affinity, we build off of the general regularized self-expression form in (1). In addition to learning a self-expressive matrix \mathbf{C} we also wish to learn a doubly stochastic affinity matrix $\mathbf{A} \in \Omega_n$. Self-expressive formulations (roughly) model $|\mathbf{C}_{ij}|$ as proportional to the likelihood that \mathbf{x}_i and \mathbf{x}_j are in the same subspace, so we desire that our normalized affinity \mathbf{A} be close to $|\mathbf{C}|$ (optionally after scaling \mathbf{A} by a constant to match the scale of $|\mathbf{C}|$), which we incorporate via the use of a penalty function $\Theta(\cdot, \cdot)$. Thus, we have a general framework:

$$\begin{aligned} \min_{\mathbf{C}, \mathbf{A}} \quad & \frac{1}{2} \|\mathbf{X} - \mathbf{XC}\|_F^2 + \lambda \theta(\mathbf{C}) + \gamma \Theta(|\mathbf{C}|, \mu \mathbf{A}) \\ \text{s.t.} \quad & \mathbf{A} \in \Omega_n, \text{diag}(\mathbf{C}) = \mathbf{0} \end{aligned} \quad (3)$$

The zero-diagonal constraint on \mathbf{C} is enforced to prevent each point from using itself in its self-representation, as this is not informative for clustering. While our framework is general, and can be used with e.g. low-rank penalties, we choose a simple mix of l_2 and l_1 regularization that is effective and admits fast algorithms. For Θ , we use an l_2 distance penalty, as l_2 projection of an affinity matrix onto the doubly stochastic matrices often improves spectral clustering performance [55] and results in desirable sparsity properties [37, 4]. As a result, our model takes the form of an

optimization problem over \mathbf{C} and \mathbf{A} :

$$\begin{aligned} \min_{\mathbf{C}, \mathbf{A}} \quad & \frac{1}{2} \|\mathbf{X} - \mathbf{XC}\|_F^2 + \frac{\eta_1}{2} \|\mathbf{C}\|_F^2 + \eta_2 \|\mathbf{A}\|_F^2 + \eta_3 \|\mathbf{C}\|_1 \\ \text{s.t.} \quad & \mathbf{A} \in \Omega_n, \text{diag}(\mathbf{C}) = \mathbf{0}, \end{aligned} \quad (4)$$

where $\eta_1, \eta_2 > 0, \eta_3 \geq 0$ are hyperparameters.

The objective (4) is not convex because of the $|\mathbf{C}|$ term in the \mathbf{C} -to- \mathbf{A} -difference loss. To alleviate this issue, we relax the problem by separating the self-expressive matrix \mathbf{C} into two nonnegative matrices $\mathbf{C}_p, \mathbf{C}_q \geq \mathbf{0}$, so that $\mathbf{C}_p - \mathbf{C}_q$ approximately takes the role of \mathbf{C} and $\mathbf{C}_p + \mathbf{C}_q$ approximately takes the role of $|\mathbf{C}|$ (with the approximation being exact if the nonzero support of \mathbf{C}_p and \mathbf{C}_q do not overlap). Thus, our convex model is given by:

$$\begin{aligned} \min_{\mathbf{C}_p, \mathbf{C}_q, \mathbf{A}} \quad & \frac{1}{2} \|\mathbf{X} - \mathbf{X}[\mathbf{C}_p - \mathbf{C}_q]\|_F^2 + \\ & \frac{\eta_1}{2} \|[\mathbf{C}_p + \mathbf{C}_q] - \eta_2 \mathbf{A}\|_F^2 + \eta_3 \|\mathbf{C}_p + \mathbf{C}_q\|_1 \\ \text{s.t.} \quad & \mathbf{A} \in \Omega_n, \mathbf{C}_p, \mathbf{C}_q \in \mathbb{R}_{\geq 0, \text{diag}=\mathbf{0}}^{n \times n} \end{aligned} \quad (5)$$

where $\mathbb{R}_{\geq 0, \text{diag}=\mathbf{0}}^{n \times n}$ is the set of $n \times n$ real matrices with non-negative entries and zero diagonal¹. This problem is now convex and can be efficiently solved to global optimality, as we discuss in Section 3.1. We refer to this model as Joint Doubly Stochastic Subspace Clustering (J-DSSC).

If the optimal \mathbf{C}_p and \mathbf{C}_q have disjoint support (where the support of a matrix is the set of indices (i, j) where the matrix is nonzero), then by solving (5) we also obtain a solution for (4), since we can take $\mathbf{C} = \mathbf{C}_p - \mathbf{C}_q$, in which case $|\mathbf{C}| = |\mathbf{C}_p - \mathbf{C}_q| = \mathbf{C}_p + \mathbf{C}_q$. However, this final equality does not hold when the optimal \mathbf{C}_p and \mathbf{C}_q have overlapping nonzero support. The following proposition shows that our relaxation (5) is equivalent to the original problem (4) for many parameter settings of (η_1, η_2, η_3) . In cases where the supports of \mathbf{C}_p and \mathbf{C}_q overlap, we can also bound the magnitude of the overlapping entries (hence guaranteeing a close approximation of the solution to (4) from solutions to (5)). A proof is given in the appendix.

Proposition 1. *Consider (5) with parameters $\eta_1 > 0$ and $\eta_2, \eta_3 \geq 0$. Let $(\mathbf{C}_p^*, \mathbf{C}_q^*, \mathbf{A}^*)$ be an optimal solution.*

- 1) *If $\eta_1 \eta_2 \leq \eta_3$, then the solution of the relaxation (5) is the same as that of (4), when taking $\mathbf{C} = \mathbf{C}_p^* - \mathbf{C}_q^*$. In particular, the supports of \mathbf{C}_p^* and \mathbf{C}_q^* are disjoint.*
- 2) *If $\eta_1 \eta_2 > \eta_3$, then the supports of \mathbf{C}_p^* and \mathbf{C}_q^* may overlap. At any index (i, j) for which $(\mathbf{C}_p^*)_{ij} > 0$ and $(\mathbf{C}_q^*)_{ij} > 0$, it holds that*

$$\max \left((\mathbf{C}_p^*)_{ij}, (\mathbf{C}_q^*)_{ij} \right) < \frac{\eta_1 \eta_2 - \eta_3}{\eta_1}. \quad (6)$$

¹Note that the l_1 norm $\|\mathbf{C}_p + \mathbf{C}_q\|_1$ can be replaced by the sum of the entries of $\mathbf{C}_p + \mathbf{C}_q$ because of the nonnegativity constraints.

2.3. Sequential Approximation: A-DSSC

To see an alternative interpretation of the model in (4), note the following by expanding the second term of (4):

$$(4) = \min_{\mathbf{C}, \mathbf{A}} \frac{1}{2} \|\mathbf{X} - \mathbf{XC}\|_F^2 + \frac{\eta_1}{2} \|\mathbf{C}\|_F^2 + \eta_3 \|\mathbf{C}\|_1 - \langle \eta_1 |\mathbf{C}|, \eta_2 \mathbf{A} \rangle + \frac{\eta_1 \eta_2^2}{2} \|\mathbf{A}\|_F^2 \quad (7)$$

s.t. $\mathbf{A} \in \Omega_n$, $\text{diag}(\mathbf{C}) = \mathbf{0}$

From this form, one can see that for an uninformative initialization of the affinity as $\mathbf{A} = \mathbf{I}$, the minimization w.r.t. \mathbf{C} takes the form of Elastic Net Subspace Clustering [52],

$$\min_{\mathbf{C}} \frac{1}{2} \|\mathbf{X} - \mathbf{XC}\|_F^2 + \frac{\eta_1}{2} \|\mathbf{C}\|_F^2 + \eta_3 \|\mathbf{C}\|_1 \quad (8)$$

s.t. $\text{diag}(\mathbf{C}) = \mathbf{0}$

Likewise, for a fixed \mathbf{C} , one can observe that the above problem w.r.t. \mathbf{A} is a special case of a quadratically regularized optimal transport problem [4, 28]:

$$\min_{\mathbf{A}} \langle -|\mathbf{C}|, \mathbf{A} \rangle + \frac{\eta_2}{2} \|\mathbf{A}\|_F^2 \quad \text{s.t. } \mathbf{A} \in \Omega_n. \quad (9)$$

Thus, η_2 controls the regularization on \mathbf{A} , with lower η_2 encouraging sparser \mathbf{A} and higher η_2 encouraging denser and more uniform \mathbf{A} . In particular, as $\eta_2 \rightarrow 0$, (9) approaches a linear assignment problem, which has permutation matrix solutions (i.e., maximally sparse solutions) [36, 17]. In contrast, as $\eta_2 \rightarrow \infty$, the optimal solution is densely connected and approaches the uniform matrix $\frac{1}{n} \mathbf{1}\mathbf{1}^\top$.

Hence, we consider an alternating minimization process to obtain approximate solutions for \mathbf{C} and \mathbf{A} , where we first initialize $\mathbf{A} = \mathbf{I}$ and solve (8) for \mathbf{C} . Then, holding \mathbf{C} fixed we solve (9) for \mathbf{A} . Taking the solution to this problem as the final affinity \mathbf{A} , we obtain our one-step approximation to J-DSSC, which we refer to as Approximate Doubly Stochastic Subspace Clustering (A-DSSC)². For this model, we develop a fast algorithm in Section 3, show state-of-the-art clustering performance in Section 4, and show empirically in the appendix that A-DSSC well approximates the optimization problem of J-DSSC.

Besides being an approximation to the joint model (5), A-DSSC also has an interpretation as a postprocessing method for certain subspace clustering methods that can be expressed as in (8), such as SSC, EnSC, and LSR [11, 52, 30]. Instead of arbitrarily making choices about how to postprocess \mathbf{A} and form the normalized Laplacian, we instead take \mathbf{A} to be doubly stochastic; as discussed above, this provides a principled means of generating an affinity \mathbf{A} that is suitably normalized for spectral clustering from a well-motivated convex optimization problem (9).

²Note that additional alternating minimization steps can also be used as (7) is convex w.r.t. \mathbf{C} if \mathbf{A} is held fixed (for any feasible \mathbf{A}) and vice-versa.

Algorithm 1 Doubly Stochastic Subspace Clustering.

Input: Data matrix \mathbf{X} , parameters η_1, η_2, η_3

Compute \mathbf{A} by J-DSSC (5) or A-DSSC (8), (9).

Apply spectral clustering on Laplacian $\mathbf{I} - \frac{1}{2}(\mathbf{A} + \mathbf{A}^\top)$.

Output: Clustering result.

Algorithm 2 Scalable A-DSSC Active-set method.

Input: Data matrix \mathbf{X} , parameters η_1, η_2, η_3

Compute \mathbf{C} in (8) by an EnSC or LSR solver.

Initialize \mathbf{S} (see appendix).

Initialize α_o and $\beta_o \in \mathbb{R}^n$.

Compute $\mathbf{A}_o = \frac{1}{\eta_2} \left[|\mathbf{C}| - \alpha_o \mathbf{1}^\top - \mathbf{1} \beta_o^\top \right]_+$.

while \mathbf{A}_o is not doubly stochastic **do**

 Compute α_o and β_o in (13) by L-BFGS.

 Compute $\mathbf{A}_o = \frac{1}{\eta_2} \left[|\mathbf{C}| - \alpha_o \mathbf{1}^\top - \mathbf{1} \beta_o^\top \right]_+$.

$\text{supp}(\mathbf{S}) \leftarrow \text{supp}(\mathbf{A}_o) \cup \text{supp}(\mathbf{S})$.

end while

Output: Optimal $\mathbf{A} = \mathbf{A}_o$.

3. Optimization and Implementation

Here we outline the optimization procedures to compute J-DSSC and A-DSSC. The basic algorithm for subspace clustering with our models is in Algorithm 1. Further algorithmic and implementation details are in the appendix.

3.1. Joint Solution for J-DSSC

In order to efficiently solve (5), we develop an algorithm in the style of linearized ADMM [31]. We reparameterize the problem by introducing additional variables, and iteratively take minimization steps over an augmented Lagrangian as well as dual ascent steps on dual variables. As this procedure is rather standard, we delegate the full description of it to the appendix.

3.2. Approximation Solution for A-DSSC

Solving for \mathbf{C} . As previously suggested, the approximate model A-DSSC can be more efficiently solved than J-DSSC. First, the minimization over \mathbf{C} in (8) can be solved by certain scalable subspace clustering algorithms. In general, it is equivalent to EnSC, for which scalable algorithms have been developed [52]. Likewise, in the special case of $\eta_1 > 0, \eta_3 = 0$, it is equivalent to LSR [30], which can be computed by a single $n \times n$ linear system solve.

Solving for \mathbf{A} . Prior work has focused on computing the doubly stochastic projection (9) through the primal [55, 37], but we will instead solve it through the dual. The dual gives an unconstrained optimization problem over two vectors $\alpha, \beta \in \mathbb{R}^n$, which is easier to solve as it eliminates the coupled constraints in the primal. We give computa-

tional evidence in the appendix that the dual allows for significantly faster computation, with over an order of magnitude improvement in certain settings. Moreover, the dual allows us to develop a highly scalable active-set method in Section 3.3, which also admits a simple GPU implementation — thus allowing for even further speed-up over existing methods. Now, the dual takes the form:

$$\max_{\alpha, \beta} -\mathbf{1}^\top (\alpha + \beta) - \frac{1}{2\eta_2} \left\| \left[|\mathbf{C}| - \alpha \mathbf{1}^\top - \mathbf{1} \beta^\top \right]_+ \right\|_F^2 \quad (10)$$

in which $[\cdot]_+$ denotes half-wave rectification, meaning that $[\mathbf{x}]_+ = \max\{\mathbf{0}, \mathbf{x}\}$, applied entry-wise. The optimal matrix \mathbf{A} is then recovered as:

$$\mathbf{A} = \frac{1}{\eta_2} \left[|\mathbf{C}| - \alpha \mathbf{1}^\top - \mathbf{1} \beta^\top \right]_+. \quad (11)$$

We use L-BFGS [26] to solve for α and β in (10).

3.3. Scalable Active-Set Method for A-DSSC

While A-DSSC can be computed more efficiently than J-DSSC, the doubly stochastic projection step still requires $\mathcal{O}(n^2)$ operations to evaluate the objective (10) and its subgradient. This limits its direct applicability to larger datasets with high n . We take advantage of the sparsity of the optimal \mathbf{A} in the parameter regimes that we choose, and develop a significantly more efficient active-set method for computing the doubly stochastic projection in (9).

Let $\mathbf{S} \in \{0, 1\}^{n \times n}$ be a binary support matrix and let \mathbf{S}^c be its complement. The basic problem that we consider is

$$\begin{aligned} \min_{\mathbf{A}} \quad & \langle -|\mathbf{C}|, \mathbf{A} \rangle + \frac{\eta_2}{2} \|\mathbf{A}\|_F^2 \\ \text{s.t.} \quad & \mathbf{A} \in \Omega_n, \mathbf{A} \odot \mathbf{S}^c = \mathbf{0}. \end{aligned} \quad (12)$$

Again, we use the dual to develop an efficient solver:

$$\begin{aligned} \max_{\alpha_o, \beta_o \in \mathbb{R}^n} \quad & -(\alpha_o + \beta_o)^\top \mathbf{1} \\ & - \frac{1}{2\eta_2} \left\| \left[|\mathbf{C}| - \alpha_o \mathbf{1}^\top - \mathbf{1} \beta_o^\top \right]_+ \odot \mathbf{S} \right\|_F^2. \end{aligned} \quad (13)$$

Here, the dual objective and its subgradient can be evaluated in $\mathcal{O}(|\mathbf{S}|)$ time, where $|\mathbf{S}|$ is the number of nonzeros in \mathbf{S} . In practice, we tend to only need $|\mathbf{S}|$ that is substantially smaller than n^2 , so this results in major efficiency increases. Also, we need only compute the elements in \mathbf{C} that are in the support \mathbf{S} ; these elements can be precomputed and stored at a low memory cost for faster L-BFGS iterations. In particular, this allows using LSR (i.e. setting $\eta_3 = 0$) in large datasets; even though the LSR \mathbf{C} is dense and takes $\mathcal{O}(n^2)$ memory, we need only compute $\mathbf{C} \odot \mathbf{S}$, which can be done efficiently with closed form matrix computations and takes $\mathcal{O}(|\mathbf{S}|)$ memory (see appendix). As stated above,

the objective and subgradient computations can be easily implemented on GPU — allowing even further speed-ups.

For a dual solution (α_o, β_o) of (13), the primal solution is $\frac{1}{\eta_2} [|\mathbf{C}| - \alpha_o \mathbf{1}^\top - \mathbf{1} \beta_o^\top]_+ \odot \mathbf{S}$. We show in the appendix that if the affinity with unrestricted support $\mathbf{A}_o = \frac{1}{\eta_2} [|\mathbf{C}| - \alpha_o \mathbf{1}^\top - \mathbf{1} \beta_o^\top]_+$ is doubly stochastic, then \mathbf{A}_o is the primal optimal solution to (9). Thus, if we iteratively update an initial support \mathbf{S} , then the row and column sums of \mathbf{A}_o provide stopping criteria that indicate optimality. On the other hand, if \mathbf{A}_o is not doubly stochastic, then the support of the true minimizer \mathbf{A} of the unrestricted problem (9) is not contained in $\text{supp}(\mathbf{S})$, so $\text{supp}(\mathbf{S})$ is too small. In this case, we update the support by $\text{supp}(\mathbf{S}) \leftarrow \text{supp}(\mathbf{A}_o) \cup \text{supp}(\mathbf{S})$.

Thus, we have an algorithm that initializes a support and then iteratively solves problems of restricted support (13) until the unrestricted affinity \mathbf{A}_o is doubly stochastic. This is formalized in Algorithm 2. The appendix discusses choices of initial support. We can prove the following correctness result:

Proposition 2. *Algorithm 2 computes an optimal \mathbf{A} for (9) in a finite number of steps.*

A proof is given in the appendix. In practice, we find that only one or two updates of the support are necessary to find the optimal \mathbf{A} , and the algorithm runs very quickly, solving problem (9) several orders of magnitude faster than previously proposed algorithms [55, 37].

4. Experiments

In this section, we empirically study our J-DSSC and A-DSSC models. We show that they achieve state-of-the-art subspace clustering performance on a variety of real datasets with multiple performance metrics. In the appendix, we provide more experiments that demonstrate additional strengths and interesting properties of our models.

4.1. Experimental Setup

Algorithms. We compare against several state-of-the-art subspace clustering algorithms, which are all affinity-based: SSC [10, 11], EnSC [52], LSR [30], LRSC [42], TSC [16], SSC-OMP [53], and S³COMP [6]. For these methods, we run the experiments on our own common framework, and we note that the results we obtain are similar to those that have been reported previously in the literature on the same datasets for these methods. We report partial results from the paper of S³COMP [6], which is included as it is a recent well-performing model. Besides TSC, which uses an inner product similarity, these methods all compute an affinity based on some self-expressive loss.

Although methods for clustering data in a union of subspaces are not directly comparable to subspace clustering neural networks [14], which cluster data supported in a

union of non-linear manifolds, we still include some comparisons. In particular, we run experiments with DSC-Net [20] as a representative neural network based method and include further comparisons (that are qualitatively similar) to other neural networks [58, 57, 56, 1] in the appendix. However, we note that recent work [14] has shown that DSC-Net (and many related works for network-based subspace clustering) are often fundamentally ill-posed, calling into question the validity of the results from these methods.

Metrics. As is standard in evaluations of clustering, we use clustering accuracy (ACC) [53] and normalized mutual information (NMI) [21] metrics, where we take the denominator in NMI to be the arithmetic average of the entropies. Also, we consider a subspace-preserving error (SPE), which is given by $\frac{1}{n} \sum_{i=1}^n \sum_{j \notin \mathcal{S}_{y_i}} |\mathbf{A}_{ij}| / \|\mathbf{A}_i\|_1$, where \mathcal{S}_{y_i} denotes the (subspace) cluster that point \mathbf{x}_i belongs to, and \mathbf{A}_i is the i th column of \mathbf{A} . This measures the proportion of mass in the affinity that is erroneously given to points in different (subspace) clusters, and is often used in evaluation of subspace clustering algorithms [53, 40]. We report the sparsity of learned affinities by the average number of nonzeros per column (NNZ). Although sparse affinities are generally preferred, the sparsest affinity is not necessarily the best.

Datasets. We test subspace clustering performance on the Extended Yale-B dataset [12], Columbia Object Image Library (COIL-40 and COIL-100) [33], UMIST face dataset [13], ORL face dataset [38], MNIST [23], and EMNIST-Letters [7]. We run experiments with the raw pixel data from the images of certain datasets; for COIL, UMIST, MNIST, and EMNIST we run separate experiments with features obtained from a scattering convolution network [5] reduced to dimension 500 by PCA [47]. This has been used in previous subspace clustering works [52, 6] to better embed the raw pixel data in a union of linear subspaces.

We do not evaluate DSC-Net [20] on scattered features as the network architecture is only compatible with image data. For MNIST ($n=70,000$) and EMNIST ($n=145,600$), we can only run scalable methods, as neural networks and other methods that form dense n -by- n matrices have unmanageable memory and runtime costs.

Clustering setup. For each baseline method we learn the \mathbf{C} from that method, form the affinity as $\hat{\mathbf{A}} = (|\mathbf{C}| + |\mathbf{C}|^\top)/2$, take the normalized Laplacian $\mathbf{L} = \mathbf{I} - \mathbf{D}^{-1/2} \hat{\mathbf{A}} \mathbf{D}^{-1/2}$ (where $\mathbf{D} = \text{diag}(\hat{\mathbf{A}}\mathbf{1})$), and then apply spectral clustering with the specified number of clusters k [43]. For our DSSC methods, we form $\hat{\mathbf{A}} = (\mathbf{A} + \mathbf{A}^\top)/2$ and use $\mathbf{L} = \mathbf{I} - \hat{\mathbf{A}}$ directly for spectral clustering (recall our affinity is invariant to Laplacian normalization). For the spectral clustering we take the k eigenvectors corresponding to the k smallest eigenvalues of \mathbf{L} as an embedding of the data (we take $k+1$ eigenvectors for MNIST as in [6], as well as for EMNIST for similar reasons). After normalizing these embeddings to

have unit l_2 norm, we obtain clusterings by random initializations of k -means clustering, compute the accuracy and NMI for each clustering, then report the average accuracy and NMI as the final result. We emphasize that for each method we obtain a nonnegative, symmetric affinity by a shared postprocessing of \mathbf{C} and/or \mathbf{A} instead of using different ad-hoc postprocessing methods that may confound the comparisons. Since DSC-Net is highly reliant on its ad-hoc postprocessing [14], we also report results with its postprocessing strategy applied (shown as DSC-Net-PP).

Parameter choices. As is often done in subspace clustering evaluation, we choose hyperparameters for each method by searching over some set of parameters and reporting the results that give the highest clustering accuracy. For DSC-Net, we use the suggested parameters in [20] where applicable, and search over hyperparameters for novel datasets. We give details on model hyperparameters in the appendix.

4.2. Results

Experimental results are reported in Tables 1 and 2. On each dataset, one of our DSSC methods achieves the highest accuracy and NMI among all non-neural-network methods. In fact, on scattered data, DSSC achieves higher accuracy and NMI than the neural method DSC-Net, even when allowing DSC-Net to use its ad-hoc postprocessing. DSC-Net with postprocessing does achieve better performance on Yale-B and ORL than our methods, though without postprocessing our models outperform it; further, note that our method is considerably simpler than DSC-Net which requires training a neural network and hence requires choices of width, activations, stochastic optimizer, depth, and so on. Moreover, our models substantially outperform DSC-Net on both the raw pixel data and scattered embeddings of UMIST, COIL-40, and COIL-100 — achieving perfect clusterings of COIL-40 and near-perfect clusterings of COIL-100 — establishing new states-of-the-art to the best of our knowledge. Likewise, among the scalable methods our models achieve very strong performance on (E)MNIST.

We also see that A-DSSC, which can be viewed as running SSC, EnSC or LSR followed by a principled doubly stochastic postprocessing, outperforms SSC, EnSC, and LSR across all datasets. This suggests that the doubly stochastic affinity matrices learned by our models are indeed effective as inputs into spectral clustering and that our method can also potentially be combined with other subspace clustering methods as a principled normalization step. Beyond clustering accuracy, our models also learn affinity matrices with other desirable properties, such as having the lowest SPE among all methods — indicating that our learned affinities place mass in the correct subspaces.

Table 1. Subspace clustering results on different datasets. ‘—’ indicates that we do not have results, and ‘N/A’ indicates that the method cannot be run for the given dataset. Best results with respect to ACC, NMI, and SPE are **bolded**.

Dataset	Metric	Shallow Affinity-Based							Neural		Doubly Stochastic	
		SSC	EnSC	LSR	LRSC	TSC	SSC-OMP	S ³ COMP	DSC-Net	DSC-Net-PP	J-DSSC	A-DSSC
Yale-B	ACC	.654	.652	.659	.662	.514	.780	.874	.691	.971	.924	.917
	NMI	.734	.734	.743	.739	.629	.844	—	.746	.961	.952	.947
	SPE	.217	.218	.869	.875	.217	.179	.203	.881	.038	.080	.080
	NNZ	22.9	23.7	2413	2414	4.3	9.1	—	2414	22.1	14.5	14.4
COIL-40	ACC	.799	.801	.577	.567	.813	.411	—	.543	.751	.899	.922
	NMI	.940	.930	.761	.736	.916	.605	—	.743	.887	.963	.967
	SPE	.013	.017	.926	.877	.057	.025	—	.873	.105	.012	.008
	NNZ	3.1	6.2	2879	2880	4.5	2.9	—	2880	13.1	8.9	5.2
COIL-40 (Scattered)	ACC	.996	.993	.734	.753	.941	.489	—	N/A	N/A	1.00	1.00
	NMI	.998	.995	.868	.871	.981	.711	—	N/A	N/A	1.00	1.00
	SPE	.0002	0.00	.787	.816	.004	.056	—	N/A	N/A	.00006	.00003
	NNZ	2.2	4.0	2879	2880	4.3	9.1	—	N/A	N/A	13.8	8.9
COIL-100	ACC	.704	.680	.492	.476	.723	.313	.789	.493	.635	.796	.824
	NMI	.919	.901	.753	.733	.904	.588	—	.752	.875	.943	.946
	SPE	.052	.044	.945	.946	.057	.052	.032	.958	.384	.049	.037
	NNZ	3.1	6.8	7199	7200	3.6	3.0	—	7200	44.7	9.9	5.8
COIL-100 (Scattered)	ACC	.954	.967	.642	.654	.915	.397	—	N/A	N/A	.961	.984
	NMI	.991	.990	.846	.850	.975	.671	—	N/A	N/A	.992	.997
	SPE	.002	.004	.891	.905	.009	.055	—	N/A	N/A	.004	.001
	NNZ	2.3	4.2	7199	7200	4.3	9.1	—	N/A	N/A	10.4	6.6
UMIST	ACC	.537	.562	.462	.494	.661	.509	—	.456	.708	.732	.725
	NMI	.718	.751	.645	.662	.829	.680	—	.611	.848	.858	.851
	SPE	.079	.085	.811	.824	.035	.091	—	.834	.393	.036	.034
	NNZ	4.9	6.6	574	575	3.7	2.9	—	575	23.2	5.1	4.8
UMIST (Scattered)	ACC	.704	.806	.524	.531	.714	.401	—	N/A	N/A	.873	.888
	NMI	.834	.903	.701	.711	.855	.510	—	N/A	N/A	.939	.935
	SPE	.038	.029	.758	.804	.030	.294	—	N/A	N/A	.020	.018
	NNZ	2.7	4.5	574	575	3.8	14.5	—	N/A	N/A	7.2	5.4
ORL	ACC	.774	.774	.709	.679	.783	.664	—	.758	.845	.785	.790
	NMI	.903	.903	.856	.834	.896	.832	—	.878	.915	.906	.910
	SPE	.240	.268	.884	.874	.272	.305	—	.885	.421	.176	.159
	NNZ	12.3	14.4	399	400	9.3	5.0	—	400	20.7	10.8	9.8

Table 2. Large-scale subspace clustering results. ‘—’ indicates that we do not have results for the method. Best results are **bolded**.

Dataset	Metric	Shallow Affinity-Based					Doubly Stochastic	
		SSC	EnSC	TSC	SSC-OMP	S ³ COMP	A-DSSC	
MNIST (Scattered)	ACC	.963	.963	.980	.574	.963	.990	
	NMI	.915	.915	.946	.624	—	.971	
	SPE	.098	.098	.028	.301	.301	.017	
	NNZ	39.3	40.2	18.1	25.4	—	14.7	
EMNIST (Scattered)	ACC	.638	.644	.698	.304	—	.744	
	NMI	.745	.746	.785	.385	—	.832	
	SPE	.173	.174	.106	.216	—	.100	
	NNZ	22.3	24.7	6.3	3.7	—	17.5	

5. Conclusion

In this work, we propose models based on learning doubly stochastic affinity matrices that unify the self-expressive modeling of subspace clustering with the subsequent spectral clustering. We develop efficient algorithms for computing our models, including a novel active-set method that is highly scalable and allows for clustering large computer vision datasets. We demonstrate experimentally that our methods achieve substantial improvements in subspace

clustering accuracy over state-of-the-art models, without using any of the ad-hoc postprocessing steps that many other methods rely on. Our work further suggests many promising directions for future research by better merging the self-expressive modeling of subspace clustering with spectral clustering (or other graph clustering).

Acknowledgements. We thank Tianjiao Ding, Charles R. Johnson, and Isay Katsman for helpful discussions. This work was partially supported by the Northrop Grumman

Mission Systems Research in Applications for Learning Machines (REALM) initiative, the Johns Hopkins University Research Experience for Undergraduates in Computational Sensing and Medical Robotics (CSMR REU) program, NSF 1704458, and NSF 1934979.

References

- [1] Mahdi Abavisani, Alireza Naghizadeh, Dimitris Metaxas, and Vishal M Patel. Deep subspace clustering with data augmentation. In *Conference on Neural Information Processing Systems (NeurIPS)*, 2020. 7, 15
- [2] Amir Adler, Michael Elad, and Yacov Hel-Or. Linear-time subspace clustering via bipartite graph modeling. *IEEE transactions on neural networks and learning systems*, 26(10):2234–2246, 2015. 3
- [3] David J Aldous. The $\zeta(2)$ limit in the random assignment problem. *Random Structures & Algorithms*, 18(4):381–418, 2001. 12
- [4] Mathieu Blondel, Vivien Seguy, and Antoine Rolet. Smooth and sparse optimal transport. In *International Conference on Artificial Intelligence and Statistics*, pages 880–889, 2018. 3, 4, 5, 12, 13
- [5] Joan Bruna and Stéphane Mallat. Invariant scattering convolution networks. *IEEE transactions on pattern analysis and machine intelligence*, 35(8):1872–1886, 2013. 7, 16
- [6] Ying Chen, Chun-Guang Li, and Chong You. Stochastic sparse subspace clustering. In *Proceedings of the IEEE/CVF Conference on Computer Vision and Pattern Recognition*, pages 4155–4164, 2020. 3, 6, 7
- [7] Gregory Cohen, Saeed Afshar, Jonathan Tapson, and Andre Van Schaik. Emnist: Extending mnist to handwritten letters. In *2017 International Joint Conference on Neural Networks (IJCNN)*, pages 2921–2926. IEEE, 2017. 7, 16
- [8] Gabriel Andrew Dirac. Some theorems on abstract graphs. *Proceedings of the London Mathematical Society*, 3(1):69–81, 1952. 12
- [9] Eva L Dyer, Aswin C Sankaranarayanan, and Richard G Baraniuk. Greedy feature selection for subspace clustering. *The Journal of Machine Learning Research*, 14(1):2487–2517, 2013. 3
- [10] Ehsan Elhamifar and René Vidal. Sparse subspace clustering. In *2009 IEEE Conference on Computer Vision and Pattern Recognition*, pages 2790–2797. IEEE, 2009. 1, 2, 6, 17
- [11] Ehsan Elhamifar and René Vidal. Sparse subspace clustering: Algorithm, theory, and applications. *IEEE transactions on pattern analysis and machine intelligence*, 35(11):2765–2781, 2013. 1, 2, 3, 4, 5, 6
- [12] Athinodoros S. Georgiades, Peter N. Belhumeur, and David J. Kriegman. From few to many: Illumination cone models for face recognition under variable lighting and pose. *IEEE transactions on pattern analysis and machine intelligence*, 23(6):643–660, 2001. 7, 15
- [13] Daniel B Graham and Nigel M Allinson. Characterising virtual eigensignatures for general purpose face recognition. In *Face Recognition*, pages 446–456. Springer, 1998. 7, 15
- [14] Benjamin Haeffele, Chong You, and Rene Vidal. A critique of self-expressive deep subspace clustering. In *International Conference on Learning Representations*, 2021. 3, 6, 7, 15
- [15] Amit Harlev, Charles R Johnson, and Derek Lim. The doubly stochastic single eigenvalue problem: A computational approach. *Experimental Mathematics*, pages 1–10, 2020. 2
- [16] Reinhard Heckel and Helmut Bölcskei. Robust subspace clustering via thresholding. *IEEE Transactions on Information Theory*, 61(11):6320–6342, 2015. 6, 17
- [17] Roger A Horn and Charles R Johnson. *Matrix analysis*. Cambridge university press, 2012. 2, 5, 12
- [18] Eric Jankowski, Charles R Johnson, and Derek Lim. Spectra of convex hulls of matrix groups. *Linear Algebra and its Applications*, 2020. 2
- [19] Pan Ji, Mathieu Salzmann, and Hongdong Li. Efficient dense subspace clustering. In *IEEE Winter Conference on Applications of Computer Vision*, pages 461–468. IEEE, 2014. 3
- [20] Pan Ji, Tong Zhang, Hongdong Li, Mathieu Salzmann, and Ian Reid. Deep subspace clustering networks. In *Advances in Neural Information Processing Systems*, pages 24–33, 2017. 3, 7, 15, 16
- [21] Tarald O Kvalseth. Entropy and correlation: Some comments. *IEEE Transactions on Systems, Man, and Cybernetics*, 17(3):517–519, 1987. 7
- [22] Boris Landa, Ronald R Coifman, and Yuval Kluger. Doubly-stochastic normalization of the gaussian kernel is robust to heteroskedastic noise. *arXiv preprint arXiv:2006.00402*, 2020. 2, 3
- [23] Yann LeCun, Léon Bottou, Yoshua Bengio, and Patrick Haffner. Gradient-based learning applied to document recognition. *Proceedings of the IEEE*, 86(11):2278–2324, 1998. 7, 16
- [24] Minsik Lee, Jieun Lee, Hyeogjin Lee, and Nojun Kwak. Membership representation for detecting block-diagonal structure in low-rank or sparse subspace clustering. In *Proceedings of the IEEE conference on computer vision and pattern recognition*, pages 1648–1656, 2015. 3
- [25] Chun-Guang Li, Chong You, and René Vidal. Structured sparse subspace clustering: A joint affinity learning and subspace clustering framework. *IEEE Transactions on Image Processing*, 26(6):2988–3001, 2017. 3
- [26] Dong C Liu and Jorge Nocedal. On the limited memory bfgs method for large scale optimization. *Mathematical programming*, 45(1-3):503–528, 1989. 6
- [27] Guangcan Liu, Zhouchen Lin, Shuicheng Yan, Ju Sun, Yong Yu, and Yi Ma. Robust recovery of subspace structures by low-rank representation. *IEEE transactions on pattern analysis and machine intelligence*, 35(1):171–184, 2012. 3
- [28] Dirk A Lorenz, Paul Manns, and Christian Meyer. Quadratically regularized optimal transport. *Applied Mathematics & Optimization*, pages 1–31, 2019. 3, 5
- [29] Canyi Lu, Jiashi Feng, Zhouchen Lin, Tao Mei, and Shuicheng Yan. Subspace clustering by block diagonal representation. *IEEE transactions on pattern analysis and machine intelligence*, 41(2):487–501, 2018. 3
- [30] Can-Yi Lu, Hai Min, Zhong-Qiu Zhao, Lin Zhu, De-Shuang Huang, and Shuicheng Yan. Robust and efficient subspace

- segmentation via least squares regression. In *European conference on computer vision*, pages 347–360. Springer, 2012. 1, 5, 6, 12, 14, 17
- [31] Shiqian Ma. Alternating proximal gradient method for convex minimization. *Journal of Scientific Computing*, 68(2):546–572, 2016. 3, 5
- [32] Behrooz Nasihatkon and Richard Hartley. Graph connectivity in sparse subspace clustering. In *CVPR 2011*, pages 2137–2144. IEEE, 2011. 2, 4
- [33] Sameer A Nene, Shree K Nayar, and Hiroshi Murase. Columbia object image library (coil-100). Technical report, Columbia University, 1996. 7, 15
- [34] Feiping Nie, Xiaoqian Wang, Michael I Jordan, and Heng Huang. The constrained laplacian rank algorithm for graph-based clustering. In *Thirtieth AAAI Conference on Artificial Intelligence*, 2016. 2, 3
- [35] Xi Peng, Lei Zhang, and Zhang Yi. Scalable sparse subspace clustering. In *Proceedings of the IEEE conference on computer vision and pattern recognition*, pages 430–437, 2013. 3
- [36] Gabriel Peyré, Marco Cuturi, et al. Computational optimal transport: With applications to data science. *Foundations and Trends® in Machine Learning*, 11(5-6):355–607, 2019. 5
- [37] Nikitas Rontsis and Paul J. Goulart. Optimal approximation of doubly stochastic matrices. In *AISTATS*, 2020. 4, 5, 6, 12, 13
- [38] Ferdinando S Samaria and Andy C Harter. Parameterisation of a stochastic model for human face identification. In *Proceedings of 1994 IEEE workshop on applications of computer vision*, pages 138–142. IEEE, 1994. 7, 16
- [39] Jianbo Shi and Jitendra Malik. Normalized cuts and image segmentation. *IEEE Transactions on pattern analysis and machine intelligence*, 22(8):888–905, 2000. 1
- [40] Mahdi Soltanolkotabi, Emmanuel J Candes, et al. A geometric analysis of subspace clustering with outliers. *The Annals of Statistics*, 40(4):2195–2238, 2012. 7
- [41] René Vidal. Subspace clustering. *IEEE Signal Processing Magazine*, 28(2):52–68, 2011. 1
- [42] René Vidal and Paolo Favaro. Low rank subspace clustering (lrsr). *Pattern Recognition Letters*, 43:47–61, 2014. 6, 17
- [43] Ulrike Von Luxburg. A tutorial on spectral clustering. *Statistics and computing*, 17(4):395–416, 2007. 1, 2, 3, 4, 7
- [44] Fei Wang, Ping Li, and Arnd Christian König. Learning a bi-stochastic data similarity matrix. In *2010 IEEE International Conference on Data Mining*, pages 551–560. IEEE, 2010. 2
- [45] Xiaoqian Wang, Feiping Nie, and Heng Huang. Structured doubly stochastic matrix for graph based clustering. In *Proceedings of the 22nd ACM SIGKDD International conference on Knowledge discovery and data mining*, pages 1245–1254, 2016. 2, 3, 14
- [46] Yining Wang, Yu-Xiang Wang, and Aarti Singh. Graph connectivity in noisy sparse subspace clustering. In *Artificial Intelligence and Statistics*, pages 538–546, 2016. 2, 4
- [47] Svante Wold, Kim Esbensen, and Paul Geladi. Principal component analysis. *Chemometrics and intelligent laboratory systems*, 2(1-3):37–52, 1987. 7
- [48] Yan Yan, Chunhua Shen, and Hanzi Wang. Efficient semidefinite spectral clustering via lagrange duality. *IEEE Transactions on image processing*, 23(8):3522–3534, 2014. 2
- [49] Zhirong Yang, Jukka Corander, and Erkki Oja. Low-rank doubly stochastic matrix decomposition for cluster analysis. *The Journal of Machine Learning Research*, 17(1):6454–6478, 2016. 3
- [50] Ming Yin, Shengli Xie, Zongze Wu, Yun Zhang, and Junbin Gao. Subspace clustering via learning an adaptive low-rank graph. *IEEE Transactions on Image Processing*, 27(8):3716–3728, 2018. 3
- [51] Chong You, Claire Donnat, Daniel P Robinson, and René Vidal. A divide-and-conquer framework for large-scale subspace clustering. In *2016 50th Asilomar Conference on Signals, Systems and Computers*, pages 1014–1018. IEEE, 2016. 3, 12
- [52] Chong You, Chun-Guang Li, Daniel P Robinson, and René Vidal. Oracle based active set algorithm for scalable elastic net subspace clustering. In *Proceedings of the IEEE conference on computer vision and pattern recognition*, pages 3928–3937, 2016. 1, 2, 3, 4, 5, 6, 7, 14, 16, 17
- [53] Chong You, Daniel Robinson, and René Vidal. Scalable sparse subspace clustering by orthogonal matching pursuit. In *Proceedings of the IEEE conference on computer vision and pattern recognition*, pages 3918–3927, 2016. 1, 2, 3, 4, 6, 7, 16, 17
- [54] Ron Zass and Amnon Shashua. A unifying approach to hard and probabilistic clustering. In *Tenth IEEE International Conference on Computer Vision (ICCV’05) Volume 1*, volume 1, pages 294–301. IEEE, 2005. 2
- [55] Ron Zass and Amnon Shashua. Doubly stochastic normalization for spectral clustering. In *Advances in neural information processing systems*, pages 1569–1576, 2007. 2, 3, 4, 5, 6, 12, 13, 14
- [56] Junjian Zhang, Chun-Guang Li, Chong You, Xianbiao Qi, Honggang Zhang, Jun Guo, and Zhouchen Lin. Self-supervised convolutional subspace clustering network. In *Proceedings of the IEEE/CVF Conference on Computer Vision and Pattern Recognition*, pages 5473–5482, 2019. 7, 15
- [57] Tong Zhang, Pan Ji, Mehrtash Harandi, Richard Hartley, and Ian Reid. Scalable deep k-subspace clustering. In *Asian Conference on Computer Vision*, pages 466–481. Springer, 2018. 7, 15
- [58] Pan Zhou, Yunqing Hou, and Jiashi Feng. Deep adversarial subspace clustering. In *Proceedings of the IEEE Conference on Computer Vision and Pattern Recognition*, pages 1596–1604, 2018. 7, 15, 16

Appendices

A. A-DSSC Details

A.1. Derivation of A-DSSC Dual

Here, we give a derivation for the dual (10) of the minimization over \mathbf{A} in A-DSSC, as well as the dual with restricted support (13). It suffices to derive the restricted support dual, as the full dual follows by setting \mathbf{S} as the all ones matrix. Now, recall that the primal problem is:

$$\arg \min_{\mathbf{A}} \langle -\eta_1 |\mathbf{C}|, \eta_2 \mathbf{A} \rangle + \frac{\eta_1 \eta_2^2}{2} \|\mathbf{A}\|_F^2 \quad \text{s.t. } \mathbf{A} \in \Omega_n, \mathbf{A} \odot \mathbf{S}^c = \mathbf{0} \quad (14)$$

$$= \arg \min_{\mathbf{A}} \langle -|\mathbf{C}|, \mathbf{A} \odot \mathbf{S} \rangle + \frac{\eta_2}{2} \|\mathbf{A} \odot \mathbf{S}\|_F^2 \quad \text{s.t. } \mathbf{A} \odot \mathbf{S} \in \Omega_n. \quad (15)$$

Introducing Lagrange multipliers α and $\beta \in \mathbb{R}^n$ for the row and column sum constraints, we have the equivalent problem:

$$\min_{\mathbf{A} \geq \mathbf{0}} \max_{\alpha, \beta \in \mathbb{R}^n} \langle -|\mathbf{C}|, \mathbf{A} \odot \mathbf{S} \rangle + \frac{\eta_2}{2} \|\mathbf{A} \odot \mathbf{S}\|_F^2 + \langle \alpha, (\mathbf{A} \odot \mathbf{S})\mathbf{1} - \mathbf{1} \rangle + \langle \beta, (\mathbf{A} \odot \mathbf{S})^\top \mathbf{1} - \mathbf{1} \rangle \quad (16)$$

As the primal problem is convex and has a strictly feasible point, strong duality holds by Slater's condition, so this is equivalent to:

$$\max_{\alpha, \beta \in \mathbb{R}^n} \min_{\mathbf{A} \geq \mathbf{0}} \langle -|\mathbf{C}|, \mathbf{A} \odot \mathbf{S} \rangle + \frac{\eta_2}{2} \|\mathbf{A} \odot \mathbf{S}\|_F^2 + \langle \alpha, (\mathbf{A} \odot \mathbf{S})\mathbf{1} - \mathbf{1} \rangle + \langle \beta, (\mathbf{A} \odot \mathbf{S})^\top \mathbf{1} - \mathbf{1} \rangle \quad (17)$$

$$= \max_{\alpha, \beta \in \mathbb{R}^n} -(\alpha + \beta)^\top \mathbf{1} + \min_{\mathbf{A} \geq \mathbf{0}} \langle -|\mathbf{C}|, \mathbf{A} \odot \mathbf{S} \rangle + \frac{\eta_2}{2} \|\mathbf{A} \odot \mathbf{S}\|_F^2 + \langle \alpha \mathbf{1}^\top + \mathbf{1} \beta^\top, \mathbf{A} \odot \mathbf{S} \rangle \quad (18)$$

Letting $\mathbf{K} = |\mathbf{C}| - \alpha \mathbf{1}^\top - \mathbf{1} \beta^\top$, the inner minimization takes the form:

$$\min_{\mathbf{A} \geq \mathbf{0}} \langle -\mathbf{K}, \mathbf{A} \odot \mathbf{S} \rangle + \frac{\eta_2}{2} \|\mathbf{A} \odot \mathbf{S}\|_F^2 \quad (19)$$

$$= \eta_2 \min_{\mathbf{A} \geq \mathbf{0}} \left\langle -\frac{1}{\eta_2} \mathbf{K}, \mathbf{A} \odot \mathbf{S} \right\rangle + \frac{1}{2} \|\mathbf{A} \odot \mathbf{S}\|_F^2 \quad (20)$$

$$= -\frac{1}{2\eta_2} \|\mathbf{K}\|_F^2 + \eta_2 \min_{\mathbf{A} \geq \mathbf{0}} \frac{1}{2} \left\| \frac{1}{\eta_2} \mathbf{K} - \mathbf{A} \odot \mathbf{S} \right\|_F^2 \quad (21)$$

$$= -\frac{1}{2\eta_2} \|\mathbf{K}\|_F^2 + \frac{1}{2\eta_2} \|\mathbf{K}_- \odot \mathbf{S}^c\|_F^2 \quad (22)$$

$$= -\frac{1}{2\eta_2} \|\mathbf{K}_+ \odot \mathbf{S}\|_F^2 \quad (23)$$

Where $[\mathbf{K}]_-$ is $\min\{\mathbf{K}, \mathbf{0}\}$ taken elementwise. Thus, the final version of the dual is

$$\max_{\alpha, \beta \in \mathbb{R}^n} -(\alpha + \beta)^\top \mathbf{1} - \frac{1}{2\eta_2} \left\| \left[|\mathbf{C}| - \alpha \mathbf{1}^\top - \mathbf{1} \beta^\top \right]_+ \odot \mathbf{S} \right\|_F^2 \quad (24)$$

and the optimal value of \mathbf{A} is as given as

$$\mathbf{A} = \frac{1}{\eta_2} \left[|\mathbf{C}| - \alpha \mathbf{1}^\top - \mathbf{1} \beta^\top \right]_+ \odot \mathbf{S} \quad (25)$$

A.2. Active-Set Method

Here, we give a proof that our active-set method in Algorithm 2 converges to an optimal solution in finitely many steps. We start with a lemma that shows the correctness of our stopping criterion.

Lemma 1. *Let \mathbf{S} contain a doubly stochastic zero-nonzero pattern in its support, and let (α_o, β_o) be a solution to the dual of the problem with restricted support (13) with parameter η_2 . Then $\mathbf{A}_o = \frac{1}{\eta_2} \left[|\mathbf{C}| - \alpha_o \mathbf{1}^\top - \mathbf{1} \beta_o^\top \right]_+$ is optimal for the original problem with unrestricted support if and only if \mathbf{A}_o is doubly stochastic.*

Proof. It is clear that any optimal solution is doubly stochastic, since these are exactly the feasibility conditions.

For the other direction, suppose that \mathbf{A}_o is doubly stochastic. Note that a subgradient of the restricted support dual objective (13) is given by:

$$\nabla_{\alpha_o} (13) = -\mathbf{1} + \frac{1}{\eta_2} \left(\left[|\mathbf{C}| - \alpha_o \mathbf{1}^\top - \mathbf{1} \beta_o^\top \right]_+ \odot \mathbf{S} \right) \mathbf{1} \quad (26)$$

$$\nabla_{\beta_o} (13) = -\mathbf{1} + \frac{1}{\eta_2} \left(\left[|\mathbf{C}| - \alpha_o \mathbf{1}^\top - \mathbf{1} \beta_o^\top \right]_+ \odot \mathbf{S} \right)^\top \mathbf{1} \quad (27)$$

In the case of unrestricted support (i.e. full support), the subgradients exactly measure how far the row sums and column sums of \mathbf{A}_o deviate from $\mathbf{1}$. Since \mathbf{A}_o is doubly stochastic, the row and column sums are $\mathbf{1}$, so the subgradients are zero. Thus, α_o and β_o are optimal for the unrestricted support dual (10), which means that we may recover the optimal primal variable as $\frac{1}{\eta_2} \left[|\mathbf{C}| - \alpha_o \mathbf{1}^\top - \mathbf{1} \beta_o^\top \right]_+$, which is exactly \mathbf{A}_o . \square

With this result, we can directly prove convergence and correctness.

Proposition 2. *Algorithm 2 computes an optimal \mathbf{A} for (9) in a finite number of steps.*

Proof. First, note that the initialization of \mathbf{S} gives a feasible problem, since the support contains a permutation matrix, which is doubly stochastic. In each iteration, we compute the matrix $\mathbf{A}_o = \frac{1}{\eta_2} \left[|\mathbf{C}| - \alpha_o \mathbf{1}^\top - \mathbf{1} \beta_o^\top \right]_+$. If \mathbf{A}_o is doubly stochastic, then we terminate and \mathbf{A}_o is optimal for the unrestricted support problem by Lemma 1. If \mathbf{A}_o is not doubly stochastic, then $\mathbf{A}_o \neq \mathbf{A}_o \odot \mathbf{S}$ since $\mathbf{A}_o \odot \mathbf{S}$ is doubly stochastic. Thus, the support is updated to a new support that has not been seen before, since it is strictly larger. There are only finitely many choices of support, so there are only finitely many iterations of this procedure, thus proving finite convergence of our algorithm. \square

A.3. Support Initialization

The primal (12) may not be feasible for certain choices of support \mathbf{S} with too many zeros, since there is not always a doubly stochastic matrix with a given zero-nonzero pattern. One would like to have an initialization for the support that is both feasible,

so that our algorithm converges, and that approximately contains the true support of the optimal \mathbf{A} , so that the convergence is fast. One reasonable guess for the support of \mathbf{A} is the top k entries of each row, since these entries contribute more to the inner product of the objective. Also, for the linear assignment problem, which is the limiting $\eta_2 = 0$ case, the top k entries of each row have been shown to contain the support of the solution \mathbf{A} with high probability [3]. However, a top k graph is not guaranteed to be feasible for reasonably sized k , as the following lemma shows:

Lemma 2. *Let n and k be integers with $n \geq k \geq 3$.*

1. *If $k < n/2$, then there exists a graph G on n nodes with minimum degree k such that there is no doubly stochastic matrix with support contained in the support of G .*
2. *If $k \geq n/2$, then there is a doubly stochastic matrix in the support of any graph on n nodes with minimum degree k .*

Proof. Let $k < n/2$, so that $n - k > k$. Consider the graph with adjacency matrix

$$\begin{bmatrix} \mathbf{0}_{n-k, n-k} & \mathbf{1}_{n-k} \mathbf{1}_k^\top \\ \mathbf{1}_k \mathbf{1}_{n-k}^\top & \mathbf{1}_k \mathbf{1}_k^\top - \mathbf{I}_{k,k} \end{bmatrix} \quad (28)$$

Each row has either k or $n - 1$ ones, so each node has at least degree k . However, there can be no permutation matrix with support contained in the support of this graph. This is because the first $n - k$ nodes only have k unique neighbors, and $n - k > k$.

Now, let $k \geq n/2$, and let G be a graph on n nodes with minimum degree $k \geq n/2$. In each connected component of the graph with m nodes, the minimum degree is at least $n/2 \geq m/2$. Thus, Dirac's theorem on Hamiltonian cycles [8] states that each connected component has a Hamiltonian cycle — a cycle that visits each node in the component. Taking the permutation matrix that is the sum of these cycles gives us a permutation matrix contained in the support of this graph, so we are done since permutation matrices are doubly stochastic. \square

One way in which the graph (28) occurs is if there is a hub and spoke structure in the graph, in which there are k closely connected nodes forming a hub and all other $n - k$ nodes are distant from each other and are connected to the k nodes in the hub. A top- k graph can certainly have this structure if \mathbf{C} is a similarity derived from some euclidean distance. In our case, \mathbf{C} is a self-expressive affinity, so it is possible that tighter bounds may be derived under some conditions, but we leave this to future work.

Choosing a top- k support initialization for some $k \geq n/2$ defeats the purpose of the active-set method, as computing a solution in this support would still require $\mathcal{O}(n^2)$ computations per iteration. In practice, we choose a small k that leads to a tractable problem size, and add some randomly sampled permutation matrices to the support to guarantee feasibility.

A.4. Self-Expressive Computation

For a general dual problem (13) with restricted support \mathbf{S} , we need only evaluate \mathbf{C}_{ij} for $(i, j) \in \text{supp}(\mathbf{S})$. These \mathbf{C}_{ij} can be computed online in each iteration if memory is an issue, or it can be precomputed and stored in $\mathcal{O}(|\mathbf{S}|)$ memory for faster objective and subgradient evaluations.

In particular, computing a subset of a dense LSR [30] solution \mathbf{C} , or computing it online allows us to scale LSR to datasets with many points like MNIST and EMNIST where the entire dense n -by- n \mathbf{C} cannot be stored. To see how this is done, note that the solution to LSR with parameter γ (i.e. a solution to (8) with $\eta_1 = \gamma, \eta_3 = 0$) with no zero diagonal constraint is given as

$$\mathbf{C} = (\mathbf{X}^\top \mathbf{X} + \gamma \mathbf{I})^{-1} \mathbf{X}^\top \mathbf{X} \quad (29)$$

The Woodbury matrix identity [17] gives that this is equal to

$$\left[\frac{1}{\gamma} \mathbf{I} - \frac{1}{\gamma^2} \mathbf{X}^\top \left(\mathbf{I} + \frac{1}{\gamma} \mathbf{X}^\top \mathbf{X} \right)^{-1} \mathbf{X} \right] \mathbf{X}^\top \mathbf{X} \quad (30)$$

$$= \frac{1}{\gamma} \mathbf{X}^\top \mathbf{X} - \frac{1}{\gamma^2} \mathbf{X}^\top \left(\mathbf{I} + \frac{1}{\gamma} \mathbf{X} \mathbf{X}^\top \right)^{-1} \mathbf{X} \mathbf{X}^\top \mathbf{X} \quad (31)$$

$$= \mathbf{X}^\top \underbrace{\left[\frac{1}{\gamma} \mathbf{I} - \frac{1}{\gamma^2} \left(\mathbf{I} + \frac{1}{\gamma} \mathbf{X} \mathbf{X}^\top \right)^{-1} \mathbf{X} \mathbf{X}^\top \right]}_{\mathbf{M}} \mathbf{X} \quad (32)$$

so we may compute $\mathbf{C}_{ij} = \mathbf{X}_i^\top \mathbf{M} \mathbf{X}_j$. Note that \mathbf{M} is d -by- d , and we do not ever need to form an n -by- n matrix in this computation.

A.5. Active-set Runtime Comparison

The computation of \mathbf{A} in A-DSSC (9) is simply application of the proximal operator for projection onto the doubly stochastic matrices Ω_n . To view it as a Frobenius-norm projection of an input matrix onto the doubly stochastic matrices, note that

$$\arg \min_{\mathbf{A} \in \Omega_n} \langle -|\mathbf{C}|, \mathbf{A} \rangle + \frac{\gamma}{2} \|\mathbf{A}\|_F^2 \quad (33)$$

$$= \arg \min_{\mathbf{A} \in \Omega_n} \left\| \frac{1}{\gamma} |\mathbf{C}| - \mathbf{A} \right\|_F^2 \quad (34)$$

In the past, algorithms for computing this have used the primal formulation. Zass and Shashua [55] use an alternating projections algorithm, while Rontsis and Goulart [37] use an ADMM based algorithm. As explained in Section 3.2, we note that the dual (10) is a special case of the dual of a regularized optimal transport problem [4], so it can be computed with the same algorithms that these regularized optimal transport problems use. Our Algorithm 2 gives a fast way to compute this dual by leveraging problem sparsity.

Here, we compare the performance of these different methods on various input matrices $|\mathbf{C}|$. The different input matrices we consider are:

- \mathcal{D}_1 , $|\mathbf{C}|$ is the A-DSSC affinity for the Yale-B dataset, so $n = 2414$.
- \mathcal{D}_2 , $|\mathbf{C}|$ is the A-DSSC affinity for scattered COIL, so $n = 7200$.
- \mathcal{D}_3 , $|\mathbf{C}|$ is $1/2(|\mathbf{G}| + |\mathbf{G}^\top|)$, scaled to have maximum element 1, where \mathbf{G} is a standard Gaussian random matrix of size 2000×2000 . We take $\gamma = .5$.
- \mathcal{D}_4 , $|\mathbf{C}|$ is an LSR affinity at $\eta_1 = 1$ for a union of ten 5-dimensional subspaces in \mathbb{R}^{15} , as in [51]. We take $n = 4000$ and $\gamma = .01$.

Table 3. Runtime (in seconds) of different doubly stochastic projection algorithms. The data \mathcal{D}_i are defined in Section A.5. “NC” indicates that the algorithm did not converge in 5000 iterations.

Method	\mathcal{D}_1	\mathcal{D}_2	\mathcal{D}_3	\mathcal{D}_4
Alt Proj [55]	NC	NC	118	264
ADMM [37]	54.1	NC	26.2	111
Dual [4]	11.8	568	1.69	13.7
Active-set (ours)	1.64	12.2	0.49	2.05

For each experiment, we run the algorithm until the row and column sums of the iterates are all within 10^{-4} of 1. Runtimes are given in Table 3. Similarly to previous work [37], we find that alternating projections has serious convergence issues; it also fails to converge to numerically sparse affinities. Our active-set method converges orders of magnitudes faster than the other methods. We emphasize that these performance gains are further amplified on larger datasets, where memory considerations can make it so that the other methods cannot even be run. Moreover, all of these experiments were run on CPU, while our method also has a GPU implementation that allows for very efficient computation on large datasets. For instance, we can compute full A-DSSC on scattered MNIST ($n = 70,000$) and achieve 99% clustering accuracy on a GeForce RTX 2080 GPU in less than 30 seconds.

B. J-DSSC Details

B.1. Linearized ADMM for J-DSSC

Algorithm 3 J-DSSC

Input: Data matrix \mathbf{X} , parameters η_1, η_2, η_3 , step sizes ρ and τ
while Not converged **do**
 Update \mathbf{C}_p and \mathbf{C}_q by linearized ADMM steps (39) to (42)
 Update \mathbf{A} , \mathbf{Y} , and \mathbf{Z} by minimization steps (43) to (47)
 Update $\lambda_1, \lambda_2, \Lambda_1$, and Λ_2 by dual ascent steps (48) to (51)
end while
Apply spectral clustering on Laplacian $\mathbf{I} - \frac{1}{2}(\mathbf{A} + \mathbf{A}^\top)$
Output: Clustering result

Here, we give details on the computation of J-DSSC by linearized ADMM. We reparameterize the problem (5) by introducing additional variables $\mathbf{Y} = \mathbf{A}$ and $\mathbf{Z} = \mathbf{X}[\mathbf{C}_p - \mathbf{C}_q]$. This gives us the equivalent problem

$$\begin{aligned}
& \min_{\mathbf{C}_p, \mathbf{C}_q, \mathbf{A}, \mathbf{Y}, \mathbf{Z}} \frac{1}{2} \|\mathbf{X} - \mathbf{Z}\|_F^2 \\
& + \frac{\eta_1}{2} \|[\mathbf{C}_p + \mathbf{C}_q] - \eta_2 \mathbf{A}\|_F^2 + \eta_3 \|\mathbf{C}_p + \mathbf{C}_q\|_1 \quad (35) \\
& \text{s.t. } \mathbf{A} \geq \mathbf{0}, \mathbf{C}_p, \mathbf{C}_q \in \mathbb{R}_{\geq 0, \text{diag}=0}^{n \times n}, \\
& \mathbf{Y}^\top \mathbf{1} = \mathbf{Y} \mathbf{1} = \mathbf{1}, \mathbf{Y} = \mathbf{A}, \mathbf{Z} = \mathbf{X}[\mathbf{C}_p - \mathbf{C}_q]
\end{aligned}$$

The augmented Lagrangian then takes the form:

$$\begin{aligned}
\mathcal{L}(\mathbf{C}_p, \mathbf{C}_q, \mathbf{A}, \mathbf{Y}, \mathbf{Z}, \lambda, \Lambda) = & \frac{1}{2} \|\mathbf{X} - \mathbf{Z}\|_F^2 \\
& + \frac{\eta_1}{2} \|[\mathbf{C}_p + \mathbf{C}_q] - \eta_2 \mathbf{A}\|_F^2 + \eta_3 \|\mathbf{C}_p + \mathbf{C}_q\|_1 \\
& + \langle \lambda_1, \mathbf{Y}^\top \mathbf{1} - \mathbf{1} \rangle + \langle \lambda_2, \mathbf{Y} \mathbf{1} - \mathbf{1} \rangle + \langle \Lambda_1, \mathbf{Y} - \mathbf{A} \rangle \quad (36) \\
& + \frac{\rho}{2} \|\mathbf{Y}^\top \mathbf{1} - \mathbf{1}\|_2^2 + \frac{\rho}{2} \|\mathbf{Y} \mathbf{1} - \mathbf{1}\|_2^2 + \frac{\rho}{2} \|\mathbf{Y} - \mathbf{A}\|_F^2 \\
& + \langle \Lambda_2, \mathbf{Z} - \mathbf{X}[\mathbf{C}_p - \mathbf{C}_q] \rangle + \frac{\rho}{2} \|\mathbf{Z} - \mathbf{X}[\mathbf{C}_p - \mathbf{C}_q]\|_F^2 \\
& + \mathcal{I}_{\geq 0}(\mathbf{A}) + \mathcal{I}_{\geq 0, \text{diag}=0}(\mathbf{C}_p) + \mathcal{I}_{\geq 0, \text{diag}=0}(\mathbf{C}_q)
\end{aligned}$$

where \mathcal{I}_S is the indicator function for the set S , which takes values of 0 in S and ∞ outside of S , and where $\rho > 0$ is a chosen constant.

In each iteration, we take a linearized ADMM step in \mathbf{C}_p and \mathbf{C}_q , then alternately minimize over \mathbf{A} , \mathbf{Y} , and \mathbf{Z} , and lastly take gradient ascent steps on each of the Lagrange multipliers. For a step size $\tau > 0$, the linearized ADMM step over \mathbf{C}_p takes the form of a gradient descent step on:

$$\begin{aligned}
h(\mathbf{C}_p) = & \langle \Lambda_2, \mathbf{Z} - \mathbf{X}[\mathbf{C}_p - \mathbf{C}_q] \rangle \\
& + \frac{\rho}{2} \|\mathbf{Z} - \mathbf{X}[\mathbf{C}_p - \mathbf{C}_q]\|_F^2, \quad (37)
\end{aligned}$$

followed by application of a proximal operator. Letting \mathbf{C}_p' be the intermediate value of \mathbf{C}_p after the gradient descent step, \mathbf{C}_p is updated as the solution to

$$\begin{aligned}
\min_{\mathbf{C}_p} \frac{\eta_1}{2} \|[\mathbf{C}_p + \mathbf{C}_q] - \eta_2 \mathbf{A}\|_F^2 + \eta_3 \|\mathbf{C}_p + \mathbf{C}_q\|_1 \\
+ \frac{1}{2\tau} \|\mathbf{C}_p' - \mathbf{C}_p\|_F^2 + \mathcal{I}_{\geq 0, \text{diag}=0}(\mathbf{C}_p) \quad (38)
\end{aligned}$$

For a matrix \mathbf{E} , let $[\mathbf{E}]_+$ be the half-wave rectification of \mathbf{E} , and let $[\mathbf{E}]_{+, d=0}$ be the matrix \mathbf{E} with all negative entries and the diagonal set to zero. Then the linearized ADMM updates are given as follows:

$$\mathbf{C}_p' \leftarrow \mathbf{C}_p - \tau \left(-\mathbf{X}^\top \Lambda_2 + \rho \mathbf{X}^\top (\mathbf{X}[\mathbf{C}_p - \mathbf{C}_q] - \mathbf{Z}) \right) \quad (39)$$

$$\mathbf{C}_p \leftarrow \left[\frac{1}{\eta_1 + \frac{1}{\tau}} \left(\frac{1}{\tau} \mathbf{C}_p' - \eta_1 \mathbf{C}_q + \eta_1 \eta_2 \mathbf{A} - \eta_3 \mathbf{1} \mathbf{1}^\top \right) \right]_{+, d=0} \quad (40)$$

$$\mathbf{C}_q' \leftarrow \mathbf{C}_q - \tau (\mathbf{X}^\top \Lambda_2 - \rho \mathbf{X}^\top (\mathbf{X}[\mathbf{C}_p - \mathbf{C}_q] - \mathbf{Z})) \quad (41)$$

$$\mathbf{C}_q \leftarrow \left[\frac{1}{\eta_1 + \frac{1}{\tau}} \left(\frac{1}{\tau} \mathbf{C}_q' - \eta_1 \mathbf{C}_p + \eta_1 \eta_2 \mathbf{A} - \eta_3 \mathbf{1} \mathbf{1}^\top \right) \right]_{+, d=0} \quad (42)$$

The sequential minimizations over \mathbf{A} then \mathbf{Y} then \mathbf{Z} , holding the other variables fixed and using the most recent value of each

variable, take the form:

$$\mathbf{A} \leftarrow \left[\frac{1}{\eta_1 \eta_2^2 + \rho} (\eta_1 \eta_2 [\mathbf{C}_p + \mathbf{C}_q] + \mathbf{A}_1 + \rho \mathbf{Y}) \right]_+ \quad (43)$$

$$\mathbf{Y} \leftarrow \frac{1}{\rho} \left[\mathbf{V} - \frac{1}{n+1} \mathbf{P} \mathbf{V} \mathbf{1} \mathbf{1}^\top - \mathbf{1} \mathbf{1}^\top \mathbf{V} \frac{1}{n+1} \mathbf{P} \right] \quad (44)$$

$$\text{where } \mathbf{V} = \rho \mathbf{A} + 2\rho \mathbf{1} \mathbf{1}^\top - \mathbf{1} \lambda_1^\top - \lambda_2 \mathbf{1}^\top - \mathbf{A}_1 \quad (45)$$

$$\mathbf{P} = \mathbf{I} - \frac{1}{2n+1} \mathbf{1} \mathbf{1}^\top \quad (46)$$

$$\mathbf{Z} \leftarrow \frac{1}{1+\rho} (\mathbf{X} - \mathbf{A}_2 + \rho \mathbf{X} [\mathbf{C}_p - \mathbf{C}_q]) \quad (47)$$

The dual ascent steps on the Lagrange multipliers take the form:

$$\lambda_1 \leftarrow \lambda_1 + \rho (\mathbf{Y}^\top \mathbf{1} - \mathbf{1}) \quad (48)$$

$$\lambda_2 \leftarrow \lambda_2 + \rho (\mathbf{Y} \mathbf{1} - \mathbf{1}) \quad (49)$$

$$\mathbf{A}_1 \leftarrow \mathbf{A}_1 + \rho (\mathbf{Y} - \mathbf{A}) \quad (50)$$

$$\mathbf{A}_2 \leftarrow \mathbf{A}_2 + \rho (\mathbf{Z} - \mathbf{X} [\mathbf{C}_p - \mathbf{C}_q]) \quad (51)$$

Thus, the full J-DSSC algorithm is given in Algorithm 3.

To derive the minimization steps for a variable \mathbf{E} that is either \mathbf{C}_p , \mathbf{C}_q , \mathbf{A} , or \mathbf{Z} , we use the method of completing the square to change the corresponding minimization into one of the form $\min_{\mathbf{E} \in S} \|\mathbf{E} - \mathbf{E}'\|_F^2$ for some feasible set S and some matrix \mathbf{E}' . For instance, in the case of \mathbf{C}_p , the set S is the set of $n \times n$ nonnegative matrices with zero diagonal, and the solution is $[\mathbf{E}']_{+, d=0}$.

To minimize over \mathbf{Y} , we use different approaches often used in dealing with row or column sum constraints [55, 45]. Define $\mathbf{V} = \rho \mathbf{A} + 2\rho \mathbf{1} \mathbf{1}^\top - \mathbf{1} \lambda_1^\top - \lambda_2 \mathbf{1}^\top - \mathbf{A}_1$. Setting the gradient of the augmented Lagrangian with respect to \mathbf{Y} equal to zero, we can show that

$$\rho \mathbf{Y} + \rho \mathbf{Y} \mathbf{1} \mathbf{1}^\top + \rho \mathbf{1} \mathbf{1}^\top \mathbf{Y} = \mathbf{V} \quad (52)$$

Multiplying both sides by $\mathbf{1}$ on the right and noting that $\mathbf{1}^\top \mathbf{1} = n$, we have

$$\rho (\mathbf{I} + n\mathbf{I} + \mathbf{1} \mathbf{1}^\top) \mathbf{Y} \mathbf{1} = \mathbf{V} \mathbf{1} \quad (53)$$

$$\rho \mathbf{Y} \mathbf{1} = (\mathbf{I} + n\mathbf{I} + \mathbf{1} \mathbf{1}^\top)^{-1} \mathbf{V} \mathbf{1} \quad (54)$$

Likewise, multiplying by $\mathbf{1}^\top$ on the left gives that

$$\rho \mathbf{1}^\top \mathbf{Y} = \mathbf{1}^\top \mathbf{V} (\mathbf{I} + n\mathbf{I} + \mathbf{1} \mathbf{1}^\top)^{-1} \quad (55)$$

We use the Woodbury matrix identity to compute the inverse

$$(\mathbf{I} + n\mathbf{I} + \mathbf{1} \mathbf{1}^\top)^{-1} = \frac{1}{n+1} \left(\mathbf{I} - \frac{1}{2n+1} \mathbf{1} \mathbf{1}^\top \right). \quad (56)$$

We define $\mathbf{P} = \mathbf{I} - \frac{1}{2n+1} \mathbf{1} \mathbf{1}^\top$, so the inverse is $\frac{1}{n+1} \mathbf{P}$. Thus, using both (54) and (55) in the left hand side of (52) gives that

$$\rho \mathbf{Y} + \frac{1}{n+1} \mathbf{P} \mathbf{V} \mathbf{1} \mathbf{1}^\top + \mathbf{1} \mathbf{1}^\top \mathbf{V} \frac{1}{n+1} \mathbf{P} = \mathbf{V} \quad (57)$$

and thus the minimizing \mathbf{Y} is given as

$$\mathbf{Y} = \frac{1}{\rho} \left[\mathbf{V} - \frac{1}{n+1} \mathbf{P} \mathbf{V} \mathbf{1} \mathbf{1}^\top - \mathbf{1} \mathbf{1}^\top \mathbf{V} \frac{1}{n+1} \mathbf{P} \right]. \quad (58)$$

C. Implementation Details

We implement J-DSSC in the Julia programming language. For A-DSSC, we have separate implementations in Julia and Python, where the Python implementation uses PyTorch for GPU computations. For the J-DSSC algorithm, we take the step sizes to be $\rho = .5$ and $\tau = .0001$ for our experiments.

C.1. Complexity Analysis

Let $\mathbf{X} \in \mathbb{R}^{d \times n}$, so there are n data points in \mathbb{R}^d . For J-DSSC, each update on \mathbf{C}_p and \mathbf{C}_q takes $\mathcal{O}(dn^2)$ operations due to matrix multiplications. Each update on \mathbf{A} and \mathbf{Y} takes $\mathcal{O}(n^2)$ operations, while each update on \mathbf{Z} takes $\mathcal{O}(dn^2)$. The dual ascent steps also take $\mathcal{O}(dn^2)$ operations in total. Thus, each iteration of the linearized ADMM part takes $\mathcal{O}(dn^2)$. We note in particular that J-DSSC does not require the solution of any linear systems or any singular value decompositions, while many other subspace clustering methods do.

For A-DSSC, solving for \mathbf{C} can be done by some efficient EnSC, SSC, or LSR solver. As discussed in Section A.4, we need only compute $\mathbf{C}_{i,j}$ for $(i,j) \in \text{supp}(\mathbf{S})$ of some support \mathbf{S} , and this can be done online or as a precomputation step. The quadratically regularized optimal transport step takes $\mathcal{O}(|\mathbf{S}|)$ operations per objective function evaluation and gradient evaluation.

The spectral clustering step requires a partial eigendecomposition of $\mathbf{I} - \frac{1}{2}(\mathbf{A} + \mathbf{A}^\top)$, although we note that in practice the \mathbf{A} that is learned tends to be sparse for the parameter settings that we choose, so we can leverage sparse eigendecomposition algorithms to compute the k eigenvectors corresponding to the smallest eigenvalues. Recall that all subspace clustering methods that use spectral clustering (which is the majority of methods) require computing an eigendecomposition of equivalent size, though not all subspace clustering affinities can leverage sparse eigendecomposition methods.

C.2. Model Selection

Our method J-DSSC has three hyperparameters η_1, η_2, η_3 to set. If we fix \mathbf{A} , the problem is simply EnSC [52]. This means that we may choose the parameters η_1 and η_3 in J-DSSC as is done in EnSC. As, noted in Section 2.2, η_2 controls the sparsity of the final \mathbf{A} , with smaller η_2 tending to give sparser \mathbf{A} . Thus, we choose η_2 such that \mathbf{A} is within a desired sparsity range. To avoid solutions that are too sparse, we can consider the number of connected components of the graph associated to the solution \mathbf{A} ; if we want to obtain k clusters, we can adjust η_2 so that the number of connected components is at most k .

The parameters for A-DSSC can be selected in an analogous manner to those of J-DSSC. Another interesting consideration is that A-DSSC does very well when $\eta_3 = 0$, meaning that there is no l_1 regularization on \mathbf{C} and thus \mathbf{C} is the solution to an LSR problem [30]. In this case, \mathbf{C} can be computed efficiently with one linear system solve, and we need only set the two parameters η_1 and η_2 .

D. Proof of Proposition 1

Proof. Suppose that there is an index (i,j) such that

$$a := (\mathbf{C}_p^*)_{ij} > 0, \quad b := (\mathbf{C}_q^*)_{ij} > 0. \quad (59)$$

Table 4. Clustering accuracy comparison with neural network models. ‘—’ indicates that we do not have results for the method. We take results directly from the corresponding papers (besides DSC-Net on UMIST, which we run). Note that this is not under our main paper evaluation framework, as we cannot control postprocessing of neural models [14].

Dataset	Neural					Doubly Stochastic	
	DSC-Net [20]	DASC [58]	kSCN[57]	S ² ConvSCN [56]	MLRDSC-DA [1]	J-DSSC (Ours)	A-DSSC (Ours)
Yale-B	.973	.986	—	.985	.992	.924	.917
COIL-100	.690	—	—	.733	.793	.961	.984
ORL	.860	.883	—	.895	.897	.785	.790
UMIST	.708	.769	—	—	—	.873	.888
MNIST	—	—	.871	—	—	—	.990

Define matrices \mathbf{C}'_p and \mathbf{C}'_q such that \mathbf{C}'_p matches \mathbf{C}^*_p at every index but (i, j) and similarly for \mathbf{C}'_q . At index (i, j) , we define

$$(\mathbf{C}'_p)_{ij} = \max(a - b, 0), \quad (\mathbf{C}'_q)_{ij} = \max(b - a, 0) \quad (60)$$

We consider the value of the expanded J-DSSC objective (7) at $(\mathbf{C}'_p, \mathbf{C}'_q, \mathbf{A}^*)$ compared to the value at $(\mathbf{C}^*_p, \mathbf{C}^*_q, \mathbf{A}^*)$. Note that $\mathbf{C}'_p - \mathbf{C}'_q = \mathbf{C}^*_p - \mathbf{C}^*_q$. Thus, there are only three summands in the objective that are different between the two groups of variables. Suppose $a \geq b$. The differences are computed as:

$$\begin{aligned} & \frac{\eta_1}{2} \|\mathbf{C}'_p + \mathbf{C}'_q\|_F^2 - \frac{\eta_1}{2} \|\mathbf{C}^*_p + \mathbf{C}^*_q\|_F^2 \\ &= \frac{\eta_1}{2} (|a - b|^2 - (a + b)^2) \\ &= -2\eta_1 ab \end{aligned} \quad (61)$$

$$\begin{aligned} & -\eta_1 \langle [\mathbf{C}'_p + \mathbf{C}'_q], \eta_2 \mathbf{A}^* \rangle + \eta_1 \langle [\mathbf{C}^*_p + \mathbf{C}^*_q], \eta_2 \mathbf{A}^* \rangle \\ &= \eta_1 \eta_2 (\mathbf{A}^*)_{ij} (-|a - b| + (a + b)) \\ &= 2\eta_1 \eta_2 (\mathbf{A}^*)_{ij} b \end{aligned} \quad (62)$$

$$\begin{aligned} & \eta_3 \|\mathbf{C}'_p + \mathbf{C}'_q\|_1 - \eta_3 \|\mathbf{C}^*_p + \mathbf{C}^*_q\|_1 \\ &= \eta_3 (|a - b| - (a + b)) \\ &= -2\eta_3 b \end{aligned} \quad (63)$$

Now, we bound the difference between the objective functions for the two variables:

$$\begin{aligned} 0 &< -2\eta_1 ab + 2\eta_1 \eta_2 (\mathbf{A}^*)_{ij} b - 2\eta_3 b \\ &\leq -2\eta_1 ab + 2\eta_1 \eta_2 b - 2\eta_3 b \end{aligned}$$

where the first bound is due to $(\mathbf{C}^*_p, \mathbf{C}^*_q, \mathbf{A}^*)$ being the optimal solution, and the upper bound is due to $(\mathbf{A}^*)_{ij} \leq 1$. From these bounds, we have that

$$b \leq a < \frac{\eta_1 \eta_2 - \eta_3}{\eta_1}. \quad (64)$$

Where we recall that we assumed $b \leq a$. A similar upper bound holds with b taking the place of a in the case where $b > a$. Now, note that $a > 0$ means that $\eta_1 \eta_2 > \eta_3$, thus proving 1) through the contrapositive. This bound clearly gives the one in (6), so we have also proven 2). \square

E. Further Experiments

E.1. Comparison with Neural Networks

In Table 4, we list the clustering accuracy of subspace clustering network models against our DSSC models. These results are

taken directly from the corresponding papers, which means that they do not follow our common evaluation framework as used in Section 4 of the main paper. Thus, the neural network methods may still use their ad-hoc postprocessing methods, which have been shown to significantly affect empirical performance [14]. Nonetheless, DSSC still significantly outperforms neural methods on COIL-100, UMIST, and MNIST. In fact, self-expressive neural models generally cannot compute clusterings for datasets on the scale of MNIST or EMNIST, as they require a dense n -by- n matrix of parameters for the self-expressive layer.

E.2. Behavior of DSSC Models

Here, we explore the quality of our approximation A-DSSC by comparing the natural extension of this approximation to multiple steps of alternating minimization over \mathbf{C} in (8) and \mathbf{A} in (9). In particular, we note that additional alternating minimization steps do not bring a significant benefit over just a single alternating minimization iteration. Figure 3 displays the results of our A-DSSC model on the UMIST face dataset [13] using the experimental setup described in Section 4.1. We see that a single alternating minimization step over \mathbf{C} then \mathbf{A} , which is equivalent to our A-DSSC model, already achieves most of the decrease in the objective (5) — giving a relative error of less than 1% compared to the global minimum obtained by the full J-DSSC solution. Moreover, the clustering accuracy is robust to additional alternating minimization steps beyond a single A-DSSC step — additional steps do not increase clustering accuracy from spectral clustering on \mathbf{A} . Also, spectral clustering on \mathbf{A} achieves much higher accuracy than spectral clustering on \mathbf{C} , thus showing the utility of the doubly stochastic model.

We also investigate the sparsity and connectivity of the affinity \mathbf{A} learned by our models. In Figure 2, we show sparsity plots of the learned matrices \mathbf{A} for J-DSSC models with varying η_2 on the first five classes on the Extended Yale-B dataset [12]. The points are sorted by class, so intra-subspace connections are on the block diagonal, and inter-subspace connections are on the off-diagonal blocks. Here, it can be seen that the sparsity level of the recovered \mathbf{A} affinity is controlled by choice of the η_2 parameter even when there is no sparse regularization on \mathbf{C} (i.e., $\eta_3 = 0$), with the number of nonzeros increasing as η_2 increases.

F. Data Details

For our experiments, recall that we run subspace clustering on the Extended Yale-B face dataset [12], Columbia Object Image Library (COIL-40 and COIL-100) [33], UMIST face dataset [13],

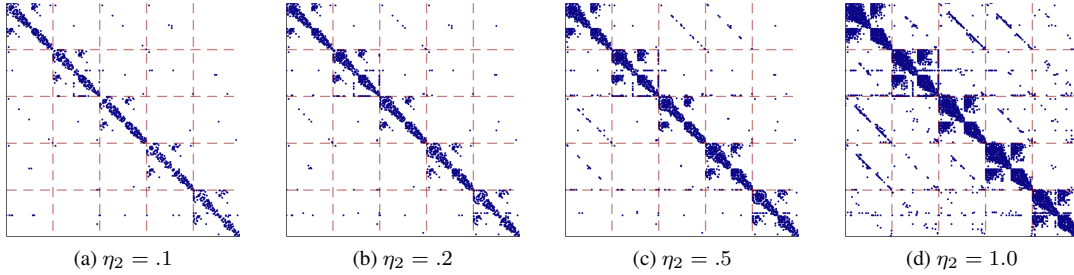


Figure 2. Affinity matrices \mathbf{A} learned by J-DSSC on the first five classes of Yale-B. We fix $\eta_1 = .25$ and $\eta_3 = 0$ (so there is no l_1 regularization on \mathbf{C}), while varying η_2 . Red dashed lines mark the boundaries between classes. Dark blue points mark nonzero entries in \mathbf{A} . The learned affinity \mathbf{A} is sparser as η_2 decreases, while it is more connected as η_2 increases.

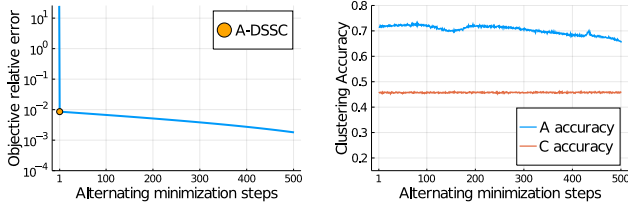


Figure 3. Objective value and clustering accuracy for different number of alternating minimization steps over \mathbf{C} in (8) then \mathbf{A} in (9) on the UMIST dataset. Our A-DSSC model is equivalent to 1 alternating minimization step. (Left) Shows relative error in the objective value compared to the true minimum. (Right) Shows clustering accuracy of using either \mathbf{A} or \mathbf{C} in spectral clustering.

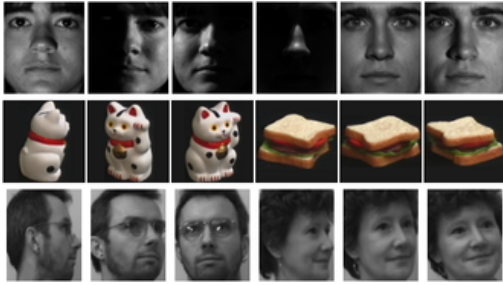


Figure 4. Sample images from Extended Yale-B (top row), COIL-100 (middle row), and UMIST (bottom row).

Table 5. Statistics and properties of datasets.

Dataset	# Images (n)	Dimension	# Classes
Yale-B	2,414	48×42	38
COIL-40	2,880	32×32	40
COIL-100	7,200	32×32	100
UMIST	575	32×32	20
ORL	400	32×32	40
MNIST	70,000	28×28	10
EMNIST	145,600	28×28	26

ORL face dataset [38], MNIST digits dataset [23], and EMNIST-Letters dataset [7]. Sample images from some of these datasets are shown in Figure 4. Basic statistics and properties of these datasets are given in Table 5.

The scattered data is computed as in [52, 53], by using a scattering convolution network [5] to compute a feature vector of 3,472 dimensions for UMIST, MNIST, and EMNIST, and $3 \cdot 3,472 = 10,416$ dimensions for COIL (since there are three color channels), then projecting to 500 dimensions by PCA. For both pixel data and scattered data, we normalize each data point to have unit l_2 norm for all experiments, noting that scaling a data point does not change its subspace membership.

For Yale-B, we remove the 18 images labeled as corrupted in the dataset, leaving 2414 images for our experiments. Adding the corrupted images back in does not appear to qualitatively change our results. We resize Yale-B to size 48×42 . The COIL, UMIST, and ORL images are resized to size 32×32 .

G. Parameter Settings

Table 6. Parameter settings for J-DSSC and A-DSSC.

Dataset	J-DSSC			A-DSSC		
	η_1	η_2	η_3	η_1	η_2	η_3
Yale-B	.25	.2	0	.5	.1	0
COIL-40	25	.01	.1	25	.001	0
COIL-40 (Scattered)	.25	.2	0	50	.001	0
COIL-100	25	.01	.1	50	.0005	0
COIL-100 (Scattered)	.25	.1	0	.1	.025	0
UMIST	1	.05	0	.5	.05	0
UMIST (Scattered)	.01	.2	0	.5	.01	0
ORL	1	.1	.1	1	.05	0
MNIST (Scattered)	N/A	N/A	N/A	10	.001	0
EMNIST (Scattered)	N/A	N/A	N/A	50	.001	0

Here, we give parameter settings for the experiments in the paper. The chosen parameter settings for our DSSC models are given in Table 6. We note that the experiments on UMIST to explore the objective value over iterations of alternating minimization in Figure 3 use the same parameter settings as in this table.

The parameters searched over for the non-neural methods are given in Table 7.

For DSC-Net, we use the hyperparameters and pre-trained autoencoders as in their original paper [20] for Yale-B, COIL-100, and ORL. For DSC-Net on UMIST, we take a similar architecture to that of [58], with encoder kernel sizes of $5 \times 5, 3 \times 3, 3 \times 3$, as well as 15, 10, 5 channels per each layer. The regularization parameters are set as $\lambda_1 = 1$ and $\lambda_2 = .2$. The DSC-Net post-

Table 7. Parameters searched over for different methods.

Method	Parameters and Variant
SSC [10]	$\gamma \in \{1, 5, 10, 25, 50, 100\}$, noisy data variant
EnSC [52]	$\gamma \in \{.1, 1, 5, 10, 50, 100\}$, $\lambda \in \{.9, .95\}$
LSR [30]	$\lambda \in \{.01, .1, .5, 1, 10, 50, 100\}$, $\text{diag}(\mathbf{C}) = \mathbf{0}$ variant
LRSC [42]	$\tau \in \{.1, 1, 10, 50, 100, 500, 1000\}$, $\alpha = \tau/2$, noisy data and relaxed constraint variant
TSC [16]	$q \in \{2, 3, \dots, 14, 15\}$
SSC-OMP [53]	$k_{\max} \in \{2, 3, \dots, 14, 15\}$
J-DSSC (Ours)	$\eta_1 \in \{.01, .25, 1, 25\}$, $\eta_2 \in \{.01, .05, .1, .2\}$, $\eta_3 \in \{0, .1\}$
A-DSSC (Ours)	$\eta_1 \in \{.1, 1, 10, 25, 50\}$, $\eta_2 \in \{.0005, .001, .01, .025, .05, .1\}$, $\eta_3 = 0$

processing on UMIST is taken to be similar to that used for ORL. For COIL-40, we use one encoder layer of kernel size 3×3 , 20 channels, and regularization parameters $\lambda_1 = 1, \lambda_2 = 100$; we also use the same postprocessing that is used for COIL-100.